Anthropogenic Secondary Organic Aerosols Contribute Substantially to Air Pollution Mortality

Benjamin A. Nault[1,2,*], Duseong S. Jo[1,2], Brian C. McDonald[2,3], Pedro Campuzano-Jost[1,2], Douglas A. Day[1,2], Weiwei Hu[1,2,**], Jason C. Schroder[1,2,***], James Allan[4,5], Donald R. Blake[6], Manjula R. Canagaratna[7], Hugh Coe[5], Matthew M. Coggon[2,3], Peter F. DeCarlo[8], Glenn S. Diskin[9], Rachel Dunmore[10], Frank Flocke[11], Alan Fried[12], Jessica B. Gilman[3], Georgios Gkatzelis[2,3,****], Jacqui F. Hamilton[10], Thomas F. Hanisco[13], Patrick L. Hayes[14], Daven K. Henze[15], Alma Hodzic[11,16], James Hopkins[10,17], Min Hu[18], L. Greggory Huey[19], B. Thomas Jobson[20], William C. Kuster[3,*****], Alastair Lewis[10,17], Meng Li[2,3], Jin Liao[13,21], M. Omar Nawaz[15], Ilana B. Pollack[22], Jeffrey Peischl[2,3], Bernhard Rappenglück[23], Claire E. Reeves[24], Dirk Richter[12], James M. Roberts[3], Thomas B. Ryerson[3,******], Min Shao[25], Jacob M. Sommers[14,26], James Walega[12], Carsten Warneke[2,3], Petter Weibring[12], Glenn M. Wolfe[13,27], Dominique E. Young[5,*******], Bin Yuan[25], Qiang Zhang[28], Joost A. de Gouw[1,2], and Jose L. Jimenez[1,2,+]

1. Department of Chemistry, University of Colorado, Boulder, Boulder, CO, USA
2. Cooperative Institute for Research in Environmental Sciences, Boulder, Colorado, USA
3. Chemical Sciences Division, NOAA Earth System Research Laboratory, Boulder, CO
4. National Centre for Atmospheric Sciences, School of Earth and Environmental Sciences, University of Manchester, Manchester, UK
5. Centre of Atmospheric Science, School of Earth and Environmental Sciences, University of Manchester, Manchester, UK
6. Department of Chemistry, University of California, Irvine, Irvine, CA, USA
7. Center for Aerosol and Cloud Chemistry, Aerodyne Research Inc., Billerica, MA, USA
8. Department of Environmental Health Engineering, Johns Hopkins University, Baltimore, MD, USA
9. NASA Langley Research Center, Hampton, Virginia, USA
10. Wolfson Atmospheric Chemistry Laboratories, Department of Chemistry, University of York, York, UK
11. Atmospheric Chemistry Observations and Modeling Laboratory, National Center for Atmospheric Research, Boulder, CO, USA
12. Institute of Arctic and Alpine Research, University of Colorado, Boulder, CO, USA
13. Atmospheric Chemistry and Dynamic Laboratory, NASA Goddard Space Flight Center, Greenbelt, MD, USA
14. Department of Chemistry, Université de Montréal, Montréal, QC, Canada
15. Department of Mechanical Engineering, University of Colorado, Boulder, Boulder, CO, USA
16. Laboratoires d'Aréologie, Université de Toulouse, CNRS, UPS, Toulouse, France
17. National Centre for Atmospheric Sciences, Department of Chemistry, University of York, York, UK
18. State Key Joint Laboratory of Environmental Simulation and Pollution Control, College of Environmental Sciences and Engineering, Peking University, Beijing, China
19. School of Earth and Atmospheric Sciences, Georgia Institute of Technology, Atlanta, Georgia, USA
20. Laboratory for Atmospheric Research, Department of Civil and Environmental Engineering, Washington State University, Pullman, WA, USA
21. Universities Space Research Association, GESTAR, Columbia, MD, USA
22. Department of Atmospheric Science, Colorado State University, Fort Collins, CO, USA
23. Department of Earth and Atmospheric Science, University of Houston, Houston, TX, USA
24. Centre for Ocean and Atmospheric Sciences, School of Environmental Sciences, University of East Anglia, Norwich, UK
25. Institute for Environmental and Climate Research, Jinan University, Guangzhou, China
26. Air Quality Research Division, Environment and Climate Change Canada, Toronto, Ontario, Canada
27. Joint Center for Earth Systems Technology, University of Maryland, Baltimore County, Baltimore, MD, USA
28. Ministry of Education Key Laboratory for Earth System Modeling, Department of Earth System Science, Tsinghua University, Beijing, China

*Now at Center for Aerosol and Cloud Chemistry, Aerodyne Research Inc., Billerica, MA, USA
**Now at State Key Laboratory at Organic Geochemistry, Guangzhou Institute of Geochemistry, Chinese Academy of Sciences, Guangzhou, China
***Now at Colorado Department of Public Health and Environment, Denver, CO, USA
****Now at Forschungszentrum Juelich GmbH, IEK-8, Juelich, Germany
*****Has retired and worked on this manuscript as an unaffiliated co-author.
******Now at Scientific Aviation, Boulder, CO, USA

*******Now at Air Quality Research Center, University of California, Davis, CA, USA

+Corresponding author: Jose L. Jimenez (jose.jimenez@colorado.edu)

Abstract

Anthropogenic secondary organic aerosol (ASOA), formed from anthropogenic emissions of organic compounds, constitutes a substantial fraction of the mass of submicron aerosol in populated areas around the world and contributes to poor air quality and premature mortality. However, the precursor sources of ASOA are poorly understood, and there are large uncertainties in the health benefits that might accrue from reducing anthropogenic organic emissions. We show that the production of ASOA in 11 urban areas on three continents is strongly correlated with the ~~anthropogenic~~ reactivity of specific anthropogenic volatile organic compounds. The differences in ASOA production across different cities can be explained by differences in the emissions of aromatics and intermediate- and semi-volatile organic compounds, indicating the importance of controlling these ASOA precursors. With an improved modeling representation of ASOA driven by the observations, we attribute 340,000 $PM_{2.5}$ premature deaths per year to ASOA, which is over an order of magnitude higher than prior studies. A sensitivity case with a more recently proposed model for attributing mortality to $PM_{2.5}$ (the Global Exposure Mortality Model) results in up~~up~~ to 900,000 deaths. A limitation of this study is the extrapolation from cities with detailed studies and regions where detailed emission inventories are available to other~~from~~ regions ~~with detailed data to others where data is not available~~ where uncertainties in emissions are larger. In addition to further development of institutional air quality management infrastructure, c~~C~~omprehensive air quality campaigns in the countries in South and Central America, Africa, South Asia, and the Middle East are needed for further progress in this area.

1. Introduction

Poor air quality is one of the leading causes of premature mortality worldwide (Cohen et al., 2017; Landrigan et al., 2018). Roughly 95% of the world's population live in areas where $PM_{2.5}$ (fine particulate matter with diameter smaller than 2.5 μm) exceeds the World Health Organization's 10 μg m^{-3} annual average guideline (Shaddick et al., 2018). This is especially true for urban areas, where high population density is co-located with increased emissions of $PM_{2.5}$ and its gas-phase precursors from human activities. It is estimated that $PM_{2.5}$ leads to 3 to 4 million premature deaths per year, higher than the deaths associated with other air pollutants (Cohen et al., 2017). More recent analysis using concentration-response relationships derived from studies of populations exposure to high levels of ambient $PM_{2.5}$ suggest the global premature death burden could be up to twice this value (Burnett et al., 2018).

The main method to estimate premature mortality with $PM_{2.5}$ is to use measured $PM_{2.5}$ from ground observations along with derived $PM_{2.5}$ from satellites to fill in missing ground-based observations (van Donkelaar et al. 2015; van Donkelaar et al. 2016). To go from total $PM_{2.5}$ to species-dependent and even sector-dependent associated premature mortality from $PM_{2.5}$, chemical transport models (CTMs) are used to predict the fractional contribution of species and/or sector (e.g., (van Donkelaar et al. 2015; Silva et al. 2016; Lelieveld et al. 2015; van Donkelaar et al. 2016). However, though CTMs may get total $PM_{2.5}$ or even total species, e.g., organic aerosol (OA), correct, the model may be getting the values right for the wrong reason (e.g., de Gouw and Jimenez, 2009; Woody et al., 2016; Murphy et al., 2017; Baker et al., 2018; Hodzic et al., 2020). This is especially important for OA in urban areas, where models have a longstanding issue under predicting secondary OA (SOA) with some instances of over predicting primary OA (POA) (de Gouw and Jimenez, 2009; Dzepina et al., 2009; Hodzic et al., 2010; Woody et al., 2016; Zhao et al., 2016a; Janssen et al., 2017; Jathar et al., 2017). Further, this bias has even been observed for highly aged aerosols in remote regions (Hodzic et al., 2020). As has been found in prior studies for urban areas (e.g., Zhang et al., 2007; Kondo et al., 2008; Jimenez et al., 2009; DeCarlo et al., 2010; Hayes et al., 2013; Freney et al., 2014; Hu et al., 2016; Nault et al., 2018; Schroder et al., 2018) and highlighted here (Fig. 1), a substantial fraction of the observed submicron PM is OA, and a substantial fraction of the OA is composed of SOA (approximately a factor of 2 to 3 higher than POA). Thus, to better understand the sources and apportionment of $PM_{2.5}$ that contributes to premature mortality, CTMs must improve their prediction of SOA versus POA, as the sources of SOA precursors and POA can be different.

~~The average measured chemical composition of submicron PM (PM_1, which typically comprises most of $PM_{2.5}$ (Wang et al., 2015)) for various megacities, urban areas, and outflow regions around the world is shown in Fig. 1. A substantial fraction of urban PM_1 is organic aerosol (OA), which is composed of primary OA (POA, organic compounds emitted directly in the particle phase) and secondary OA (SOA, formed from chemical reactions of precursor organic gases). SOA is typically a factor of 2 to 3 higher than POA for these locations.~~

However, ~~U~~understanding the gas-phase precursors of photochemically-produced anthropogenic SOA (ASOA, defined as the photochemically-produced SOA formed from the photoxidation of anthropogenic volatile organic compounds (AVOC) (de Gouw et al., 2005; DeCarlo et al., 2010)) quantitatively is challenging (Hallquist et al., 2009). Note, for the rest of the paper, unless explicitly stated otherwise, ASOA refers to SOA produced from the photoxidation of AVOCs, as there are potentially other relevant paths for the production of SOA in urban environments (e.g., (Petit et al. 2014; Kodros et al. 2020; Kodros et al. 2018; Stavroulas et al. 2019)). Though the enhancement of ASOA is largest in large cities, these precursors and production of ASOA should be important in any location impacted by anthropogenic emissions (e.g., Fig. 1). ASOA comprises a wide range of condensable products generated by numerous chemical reactions involving AVOC precursors (Hallquist et al., 2009; Hayes et al., 2015; Shrivastava et al., 2017). The number of AVOC precursors, as well as the role of "non-traditional" AVOC precursors, along with the condensable products and chemical reactions, compound to lead to differences in the observed versus predicted ASOA for various urban environments (e.g., (de Gouw and Jimenez 2009; Dzepina et al. 2009; Hodzic et al. 2010; Woody et al. 2016; Janssen et al. 2017; Jathar et al. 2017; McDonald et al. 2018)). One solution to improve the prediction in CTMs is to use a simplified model, where lumped ASOA precursors react, non-reversibly, at a given rate constant, to produce ASOA (Hodzic and Jimenez 2011; Hayes et al. 2015; Pai et al. 2020). This simplified model has been found to reproduce the observed ASOA from some urban areas (Hodzic and Jimenez 2011; Hayes et al. 2015) but issues in other urban areas (Pai et al. 2020). This may stem from the simplified model being parameterized to two urban areas (Hodzic and Jimenez 2011; Hayes et al. 2015). These inconsistencies impact the model predicted fractional contribution of ASOA to total $PM_{2.5}$ and thus the ability to understand the source attribution to $PM_{2.5}$ and premature deaths. ~~These condensable products include intermediate volatile organic compounds (IVOCS, less volatile than traditional VOCs and often not measured or considered (Robinson et al., 2007; Hayes et al., 2015)) and semi-volatile organic compounds (SVOCs, less volatile than IVOC and similarly not measured or considered).~~

The main categories of gas-phase precursors that dominate ASOA have been the subject of intensive research. The debate on what dominates can in turn impact the understanding of what precursors to regulate to reduce ASOA, to improve air quality, and to reduce premature mortality associated with ASOA. Transportation-related emissions (e.g., tailpipe, evaporation, refueling) were assumed to be the major precursors of ASOA, which was supported by field studies (Parrish et al., 2009; Gentner et al., 2012; Warneke et al., 2012; Pollack et al., 2013). Yet, budget closure of observed ASOA mass concentrations could not be achieved with transportation-related VOCs (Ensberg et al., 2014). The contribution of urban-emitted biogenic precursors to SOA in urban areas is typically small. ~~, and rather, the contribution of b~~Biogenic SOA (BSOA) in urban areas ~~is~~ typically results from ~~dominated by regionally advected~~ advection of regional background concentrations rather than processing of locally emitted biogenic VOCs~~SOA background~~ (e.g., Hodzic et al., 2009, 2010a; Hayes et al., 2013; Janssen et al., 2017). BSOA is thought to dominate globally (Hallquist et al., 2009), but as shown in Fig. 1, the contribution of BSOA (1% to 20%) to urban concentrations, while often substantial, is typically smaller than that of ASOA (17% to 39%) (see Sect. S3.1~~2~~).

Many of these prior studies generally investigated AVOC with high volatility, where volatility here is defined as the saturation concentration, C*, in µg m^{-3} (de Gouw et al., 2005; Volkamer et al., 2006; Dzepina et al., 2009; Freney et al., 2014; Woody et al., 2016). More recent studies have identified lower volatility compounds in transportation-related emissions (e.g., Zhao et al., 2014, 2016b; Lu et al., 2018). These compounds have been broadly identified as intermediate-volatile organic compounds (IVOCs) and semi-volatile organic compounds (SVOCs). IVOCs have a C* generally of 10^{3} to 10^{6} µg m^{-3} while SVOCs have a C* generally of

1 to 10^2 µg m^{-3}. Due to their lower volatility and functional groups, these classes of compounds generally form ASOA more efficiently than traditional, higher volatile AVOCs; however, S/IVOCs have also been more difficult to measure (e.g., Zhao et al., 2014; Pagonis et al., 2017; Deming et al., 2018). IVOCs generally have been the more difficult of the two classes to measure and identify as these compounds cannot be collected onto filters to be sampled off-line (Lu et al., 2018) and generally show up as unresolved complex mixture for in-situ measurements using gas-chromatography (GC) (Zhao et al., 2014). SVOCs, on the other hand, can be more readily collected onto filters and sampled off-line due to their lower volatility (Lu et al., 2018). Another potential issue has been an under-estimation of the S/IVOC aerosol production, as well as an under-estimation in the contribution of photochemically produced S/IVOC from photooxidized "traditional" VOCs, due to partitioning of these low volatile compounds to chamber walls and tubing (Krechmer et al., 2016; Ye et al., 2016; Liu et al., 2019). Accounting for this under-estimation increases the predicted ASOA (Ma et al. 2017). The inclusion of these classes of compounds have led to improvement in some urban SOA budget closure; however, many studies still have indicated a general short-fall in ASOA budget even when including these compounds from transportation-related emissions. (Dzepina et al., 2009; Tsimpidi et al., 2010; Hayes et al., 2015; Cappa et al., 2016; Ma et al., 2017; McDonald et al., 2018).

Recent studies have indicated that emissions from volatile chemical products (VCPs), defined as pesticides, coatings, inks, adhesives, personal care products, and cleaning agents (McDonald et al., 2018), as well as cooking emissions (Hayes et al., 2015), asphalt emissions (Khare et al., 2020), and solid fuel emissions from residential wood burning and/or cookstoves (e.g., Hu et al., 2013, 2020; Schroder et al., 2018), are important. While total amounts of ASOA precursors released in cities have dramatically declined (largely due to three-way catalytic converters in cars (Warneke et al., 2012; Pollack et al., 2013; Zhao et al., 2017; Khare and Gentner, 2018)), VCPs have not declined as quickly (Khare and Gentner, 2018; McDonald et al., 2018). Besides a few cities in the US (Coggon et al., 2018; Khare and Gentner, 2018; McDonald et al., 2018), extensive VCP emission quantification has not yet been published.

Due to the uncertainty on the emissions of ASOA precursors and on the amount of ASOA formed from them, the number of premature deaths associated with urban organic emissions is largely unknown. Since numerous studies have shown the importance of VCPs and other non-traditional VOC emission sources, efforts have been made to try to improve the representation and emissions of VCPs (Seltzer et al. 2020), which can reduce the uncertainty in ASOA precursors and the associated premature deaths estimations. Currently, most studies have not included ASOA realistically (e.g., Lelieveld et al., 2015; Silva et al., 2016; Ridley et al., 2018) in source apportionment calculations of the premature deaths associated with long-term exposure of $PM_{2.5}$. These models represented total OA as non-volatile POA and “traditional” ASOA precursors (transportation-based VOCs), which largely under-predict ASOA (Ensberg et al., 2014; Hayes et al., 2015; Nault et al., 2018; Schroder et al., 2018) while over-redicting POA (e.g., (Hodzic et al. 2010; Zhao et al. 2016; Jathar et al. 2017). ~~given that the~~ This does not reflect the current understanding ~~is~~ that POA is volatile and contributes to ASOA mass concentration (e.g., Grieshop et al., 2009; Lu et al., 2018). Though the models are estimating total OA correctly (Ridley et al. 2018; Hodzic et al. 2020; Pai et al. 2020), the attribution of premature deaths to POA instead of SOA formed from “traditional” and “non-traditional” sources, including IVOCs from both sources, could lead to regulations that may not target the emissions that would reduce OA in urban areas. As PM_1 and SOA mass are highest in urban areas (Fig. 1), also shown in Jimenez et al. (2009), it is necessary to quantify the amount and identify the sources of ASOA to target future emission standards that will optimally improve air quality and the associated health impacts. As these emissions are from human activities, they will contribute to SOA mass outside urban regions and to potential health impacts outside urban regions as well. Though there are potentially other important exposure pathways to PM that may increase premature mortality, such as exposure to solid-fuel emissions indoors (e.g., Kodros et al., 2018), the focus of this paper is on exposure to outdoor ASOA and its associated impacts to premature mortality.

Here, we investigate the factors that control ASOA using 11 major urban, including megacities, field studies (Fig. 1 and Table 1). The empirical relationships and numerical models are then used to quantify the attribution of premature mortality to ASOA around the world, using the observations to improve the modeled representation of ASOA. The results provide insight into the importance of ASOA to global premature mortality due to $PM_{2.5}$ and further understanding of the~~understanding the~~ precursors and sources of ASOA in urban regions.

2. Methods

Here, we introduce the ambient observations from various campaigns used to constrain ASOA production (Sect. 2.1), description of the simplified model used in CTMs to better predict ASOA (Sect. 2.2), and description of how premature mortality was estimated for this study (Sect. 2.3). In the SI, the following can be found: description of the emissions used to calculate the ASOA budget for five different locations (Sect. S1), description of how the ASOA budget was calculated for the five different locations (Sect. S2), description of the CTM (GEOS-Chem) used in this study (Sect. S3 - S4), and error analysis for the observations (Sect. S5).

2.1 Ambient Observations

For values not previously reported in the literature (Table S4), observations taken between 11:00 – 16:00 local time were used to determine the slopes of SOA versus formaldehyde (HCHO) (Fig. S1~~2~~), peroxy acetyl nitrate (PAN) (Fig. S2~~3~~), and O_x ($O_x = O_3 + NO_2$) (Fig. S3~~4~~). For CalNex, there was an approximate 48% difference between the two HCHO measurements (Fig. S4~~1~~). Therefore, the average between the two measurements were used in this study, similar to what has been done in other studies for other gas-phase species (Bertram et al., 2007). All linear fits, unless otherwise noted, use the orthogonal distance regression fitting method (ODR).

For values in Table S4 through Table S8 not previously reported in the literature, the following procedure was applied to determine the emissions ratios, similar to the methods of Nault et al. (2018). An OH exposure ($OH_{exp} = [OH]\times\Delta t$), which is also the photochemical age (PA), was estimated by using the ratio of NO_x/NO_y (Eq. 1) or the ratio of m+p-xylene/ethylbenzene (Eq. 2). For the m+p-xylene/ethylbenzene, the emission ratio (Table S5) was determined by determining the average ratio during minimal photochemistry, similar to prior studies (de Gouw et al., 2017). This was done for only one study, TexAQS 2000. This method could be applied in that case as it was a ground campaign that operated both day and night; therefore, a ratio at night could be determined when there was minimal loss of both VOCs. The average emission ratio for the other VOCs was determined using Eq. 3 after the

OH_{exp} was calculated in Eq. 1 or Eq. 2. The rate constants used for determining OH_{exp} and emission ratios are found in Table S12~~1~~.

$$OH_{exp} = [\mathrm{OH}] \times t = \ln\left(\frac{\left(\frac{[\mathrm{NO_x}]}{[\mathrm{NO_y}]}\right)}{k_{\mathrm{OH+NO_2}}}\right) \qquad \text{Eq. 1}$$

$$OH_{exp} = [\mathrm{OH}] \times t = -\frac{1}{k_{m+p-xylene} - k_{ethylbenzene}} \times \ln\left(\frac{[\mathrm{m+p-xylene}]_t}{[ethylbenzene]_t} - \frac{[m+p-xylene]_0}{[ethylbenzene]_0}\right) \qquad \text{Eq. 2}$$

$$\frac{[\mathrm{VOC(i)}]}{[\mathrm{CO}]}(0) = -\frac{[\mathrm{VOC(i)}]}{[\mathrm{CO}]}(t) \times \left(1 - \frac{1}{exp\left(-k_i \times [\mathrm{OH}]_{exp} \times t\right)}\right) \times k_i + \frac{[\mathrm{VOC(i)}]}{[\mathrm{CO}]}(t) \times k_i \qquad \text{Eq. 3}$$

2.2 Updates to the SIMPLE Model

With the combination of the new dataset, which expands across urban areas on three continents, the SIMPLE parameterization for ASOA (Hodzic and Jimenez, 2011) is updated in the standard GEOS-Chem model to reproduce observed ASOA in Fig. 2a. The parameterization operates as represented by Eq. 4.

$$\boxed{\mathrm{Emissions} \rightarrow \mathrm{SOAP} \xrightarrow{\mathrm{k} \times [\mathrm{OH}]} \mathrm{ASOA}} \qquad \text{Eq. 4}$$

SOAP represents the lumped precursors of ASOA, k is the reaction rate coefficient with OH (1.25×10^{-11} cm^3 $molecules^{-1}$ s^{-1}), and [OH] is the OH concentration in molecules cm^{-3}. This rate constant is also consistent with observed ASOA formation time scale of ~1 day that has been observed across numerous studies (e.g., de Gouw et al., 2005; DeCarlo et al., 2010; Hayes et al., 2013; Nault et al., 2018; Schroder et al., 2018).

SOAP emissions were calculated based on the relationship between ΔSOA/ΔCO and $R_{aromatics}/\Delta CO$ in Fig. 2a. First, we calculated $R_{aromatics}/\Delta CO$ (Eq. 5) for each grid cell and time step as follows:

$$\boxed{\frac{R_{aromatics}}{\Delta CO} = \frac{E_B \times k_B + E_T \times k_T + E_X \times k_X}{E_{CO}}} \qquad \text{Eq. 5}$$

Where E and k stand for the emission rate and reaction rate coefficient with OH, respectively, for benzene (B), toluene (T), and xylenes (X). Ethylbenzene was not included in this calculation because its emission was not available in HTAPv2 emission inventory. However, ethylbenzene contributed a minor fraction of the mixing ratio (~ 7%, Table S5) and reactivity (~6%) of the total BTEX across the campaigns. Reaction rate constants used in this study were 1.22×10^{-12}, 5.63×10^{-12}, and 1.72×10^{-11} cm^3 $molec.^{-1}$ s^{-1} for benzene, toluene, and xylene, respectively (Atkinson and Arey, 2003; Atkinson et al., 2006). The $R_{aromatics}/\Delta CO$ allows a dynamic calculation of the E(VOC)/E(CO) = SOA/ΔCO. Hodzic and Jimenez (2011) and Hayes et al. (2015) used a constant value of 0.069 g g^{-1}, which worked well for the two cities investigated, but not for the expanded dataset studied here. Thus, both the aromatic emissions and CO emissions are used in this study to better represent the variable emissions of ASOA precursors (Fig. S5).

Second, E_{SOAP}/E_{CO} can be obtained from the result of Eq. 6, using slope and intercept in Fig. 2a, with a correction factor (F) to consider additional SOA production after 0.5 PA equivalent days, since Fig. 2a shows the comparison at 0.5 PA equivalent days.

$$\boxed{\frac{E_{SOAP}}{E_{CO}} = \left(Slope \times \frac{R_{Aromatics}}{\Delta CO} + Intercept \right) \times F} \qquad \text{Eq. 6}$$

Where slope is 24.8 and intercept is –1.7 from Fig. 2a. F (Eq. 7) can be calculated as follows:

$$F = \frac{ASOA_{t=\infty}}{ASOA_{t=0.5d}} = \frac{SOAP_{t=0}}{SOAP_{t=0} \times (1 - exp(-k \times \Delta t \times [OH]))}, \Delta t = 43200\ s \quad \text{Eq. 7}$$

F was calculated as 1.8 by using [OH] = 1.5 × 10^{6} molecules cm^{-3}, which was used in the definition of 0.5 PA equivalent days for Fig. 2a.

Finally, E_{SOAP} can be computed by multiplying CO emissions (E_{CO}) for every grid point and time step in GEOS-Chem by the E_{SOAP}/E_{CO} ratio.

~~2.2 Error Analysis of Observations~~

~~The errors that will be discussed here are in reference to Fig. 5 and Fig. 6 and Table S4 either come from the 1σ uncertainty in the slopes (the SOA versus~~ ~~O_x~~~~, HCHO, or PAN values) or propagation of uncertainty in observations. For SOA, we estimate the 1σ uncertainty of ~15%, which is lower than the typical 1σ uncertainty of the AMS (Bahreini et al., 2009) due to the careful calibrations and excellent intercomparisons in the various campaigns (see Table 1 for references for the AMS comparisons). For ΔCO, the largest uncertainty is associated with the CO background (Hayes et al., 2013; Nault et al., 2018), and is estimated to be ~10% at 0.5 photochemical equivalent days (Hayes et al., 2013). The uncertainty in the emission ratios is ~10% (Wang et al., 2014; de Gouw et al., 2017); though, it may be higher for the values calculated here (see above) due to the uncertainty in CO background, rate constants, and photochemical age. Therefore, for Fig. 5a, the uncertainty in the y-values is 18% and the uncertainty in the x-values is 10%. For Fig. 6, the uncertainty in the measurement is 21%.~~

~~Another potential source of uncertainty may stem from the fit of the data in Fig. 5a, as the data point from Seoul (KORUS-AQ) could be impacting the fit due to the difference in its value compared to the other locations. A sensitivity analysis, where one study was removed and a new fit was derived, was conducted to determine the impact of any one study on the fit reported in Fig. 5a (see Table S10). We find that though removing the Seoul data point increases the slope, the value is still within the uncertainty and statistically significant at the 95% confidence interval. Thus, the data from Seoul does not change the results and conclusions reported in this study.~~

~~2.3 Emission Inventories for Various Urban Areas around the World~~

~~All BTEX (benzene, toluene, ethylbenze, and xylenes) and non-BTEX aromatic emissions are shown in Table S5 (BTEX) or Table S8 (non-BTEX aromatics) and are described above. The emission ratios are derived from ambient measurements utilizing photochemical aging techniques (Nault et al., 2018).~~

~~Details of the emission inventories for cities in the US, for Beijing, and for London/UK used here to estimate the IVOC:BTEX emission ratio (Fig. 2) and thus the IVOC emissions can be found in SI Sect. 1 through 3. Briefly, emissions for the US are based on McDonald et al. (2018), for China on the Multi-resolution Emission Inventory for China (MEIC) (Zhang et al., 2009; Zheng et al., 2014, 2018; Liu et al., 2015; Li et al., 2017, 2019), and for the UK on the National Atmospheric Emissions Inventory (NAEI) (EMEP/EEA, 2016). The IVOC:BTEX emission ratio from inventories are multiplied with the observed BTEX measured in urban air to estimate IVOCs emitted in each region (Table S5), including North America, Europe, and Asia.~~

~~This ensures IVOC emissions used in our calculations properly reflect differences in mixtures of emission sources (e.g., mobile sources versus VCPs) that vary by continent for each field campaign. Additionally, we rely on inventories for estimating atmospheric abundances of IVOCs because it has been challenging to measure the full range of IVOC precursors that are emitted into urban air (Zhao et al., 2014, 2017; Lu et al., 2018). In particular, many of the IVOCs emitted from VCPs are oxygenated, which are challenging to measure using traditional gas chromatography-mass spectrometry (GC-MS) techniques. Oxygenated IVOCs may not elute completely through a non-polar column, and are likely underestimated (Zhao et al., 2014). The bottom-up IVOC:BTEX ratios for the US, Beijing, and UK are described in greater detail in SI Sect. S1 through S3. IVOC emissions are classified based on their vapor pressure (effective saturation concentration: $0.3 < C^* < 3 \times 10^6$ μg m^{-3}), with the vapor pressure estimated by the SIMPOL.1 model (Pankow and Asher, 2008). Unspeciated mass has been suggested as important SOA precursors from gasoline and diesel engines, and parameterized by n-tridecane and n-pentadecane, respectively (Jathar et al., 2014). For VCPs, the volatility distribution of VOCs is in-between that of gasoline and diesel fuel. Therefore, n-tetradecane was suggested as a surrogate for unspeciated mass of VCPs by McDonald et al. (2018).~~¶

~~Similar to IVOCs, the ability to measure the full range of SVOCs emitted into urban air is challenging. Therefore, we estimate SVOC emission ratios relative to POA mass concentrations (Table S9), as described by Ma et al. (2017). For the hydrocarbon-like portion, we used the volatility distribution from Worton et al. (2014) to estimate SVOC, as this is associated with fossil fuel emissions from transportation (Zhang et al., 2005). For the other POA, we used the~~

~~volatility distribution from Robinson et al. (2007), as this POA is typically cooking primary aerosol.~~

~~Fig. 3 shows the calculated emission ratio versus saturation concentration (c*) for the cities with emission inventories. The saturation concentration for SVOC was determined as part of the estimation procedure discussed above. For IVOC, the emission ratios for the different sources (gasoline, diesel, other fossil fuel sources, and VCP emissions) were split into the volatility bins, as in McDonald et al. (2018). Finally, for BTEX and non-BTEX aromatics, and other VOC emission ratios (see Fig. 3 for references for the other VOC emission ratios), CRC (Rumble, 2019) or SIMPOL.1 (Pankow and Asher, 2008) (for estimating vapor pressures not in CRC) was used to estimate the saturation concentrations.~~

~~2.4 ASOA Budget Analysis of Ambient Observations~~

~~To calculate the ASOA budget, we used the observed BTEX (Table S5) and non-BTEX aromatic (Table S8) emission ratios, the emission inventories for IVOC (see above), and estimated SVOCs from the primary OA emissions (see above). The methods to calculate ASOA from emissions have been described in detail elsewhere (Hayes et al., 2015; Ma et al., 2017; Schroder et al., 2018), and are briefly described here. All calculations described were conducted with the KinSim v4.02 chemical kinetics simulator (Peng and Jimenez, 2019) within Igor Pro 7 (Lake Oswego, Oregon), and are summarized in Fig. S5. A typical average particle diameter for urban environments of ~200 nm (Seinfeld and Pandis, 2006) is used to estimate the condensational sink term for the partitioning of gas-to-particle, although condensation is always fast compared to the experiment timescales. Further, we assume an average 250 g mol^{-1} molar~~

~~mass for OA and an average SOA density of 1.4 g cm^{-3} (Vaden et al., 2011; Kuwata et al., 2012). Finally, all models are initialized with the campaign specific OA background (typically ~2 μg sm^{-3}) and POA (Table S9) for partitioning of gases to the particle phase, and ran at the average temperature for the campaign.~~¶

~~For the modeled VOCs (BTEX and non-BTEX aromatics), each species undergoes temperature-dependent OH oxidation (Table S11), forming four SVOCs that partition between gas- and particle-phase, using updated SOA yields that account for wall loss (Ma et al., 2017). For IVOCs, the emission weighted SOA yields and rate constants from the "Zhao" option (Zhao et al., 2014) of Ma et al. (2017) are used, and the products are apportioned into three SVOC bins and one low-volatility organic compound (LVOC) bin (Fig. S5). Finally, SVOCs undergo photooxidation at a rate of 4×10^{-11} cm^{3} molecules^{-1} s^{-1} (Dzepina et al., 2009; Hodzic et al., 2010b; Tsimpidi et al., 2010; Hodzic and Jimenez, 2011; Hayes et al., 2015; Ma et al., 2017; Schroder et al., 2018), producing one product per oxidation step, with yields from Robinson et al. (2007) for cooking and other SVOCs and yields from Worton et al. (2014) for fossil fuel related SVOCs, as recommended by Ma et al. (2017). The products from SVOC and IVOC oxidation are allowed to further oxidize, as highlighted in Fig. S5 and described in prior studies (Hayes et al., 2015; Ma et al., 2017; Schroder et al., 2018). Generally, each product reacts at a rate of 4×10^{-11} cm^{3} molecules^{-1} s^{-1} to produce some product at one volatility bin lower, adding one oxygen to the compound for each oxidation (Dzepina et al., 2009; Tsimpidi et al., 2010; Hodzic and Jimenez, 2011; Hayes et al., 2015; Ma et al., 2017; Schroder et al., 2018). An update includes fragmentation for a fraction of the molecules that are oxidized, as described in Schroder et al. (2018) and Koo et al. (2014). As shown in Fig. S5, fragmentation of the compound occurs as it is~~

~~oxidized and goes down one volatility bin. For further oxidation of SVOCs from the oxidation of primary IVOCs, one oxygen is added and 0.25 carbon is removed per step, leading to an increase in mass of 1.03 (instead of 1.07) per oxidation step (Koo et al., 2014; Schroder et al., 2018). For further oxidation of products from primary SVOC emissions, one oxygen is added and 0.5 carbon is removed per step, leading to an increase in mass of 0.99 (instead of 1.07) per oxidation step (Koo et al., 2014; Nault et al., 2018).~~

~~2.5 GEOS-Chem Modeling~~

~~The model used in this study, for ASOA apportionment (Fig. 1), for apportionment of ASOA to total PM2.5 for premature mortality calculations (Worldwide Premature Deaths Due to ASOA), and for sensitivity analysis for ASOA production and emissions on premature mortality calculations, is the GEOS-Chem v12.0.0 global chemical transport model (Bey et al., 2001; The International GEOS-Chem User Community, 2018) to calculate global concentrations of $PM_{2.5}$ and ASOA at 2°×2.5° horizontal resolution. Goddard Earth Observing System – Forward Processing (GEOS-FP) assimilated data from the NASA Global Modeling and Assimilation Office (GMAO) were used for input meteorological fields. The model was run for 2013 to 2018 to take into account interannual variability of meteorological impacts onto $PM_{2.5}$ (therefore, averaging $PM_{2.5}$ over variations in meteorology). However, the HTAPv2 emission inventory, which was used for anthropogenic emissions (Janssens-Maenhout et al., 2015), was kept constant for the 5 years. GEOS-Chem simulates gas and aerosol chemistry with ~700 chemical reactions. GEOS-Chem calculates the following $PM_{2.5}$ species: sulfate, ammonium, nitrate (Park et al., 2006); black carbon and POA (Park et al., 2005); SOA (Pye and Seinfeld, 2010; Marais et al.,~~

2016); sea salt (accumulation mode only (Jaeglé et al., 2011)); and, dust (Duncan Fairlie et al., 2007).

2.5.1 Biogenic SOA

For monoterpene and sesquiterpene SOAs, we used the default complex SOA scheme (without semi-volatile POA) using the two-product model framework (Pye and Seinfeld, 2010). This scheme calculates initial oxidation of VOCs with OH, O_3, and NO_3, and resulting products are assigned to four different gas-phase semi-volatile species (TSOA0–3) based on volatilities (c^* = 0.1, 1, 10, 100 µg m^{-3}). Aerosol and gas species fractions are calculated online using the partitioning theory, and all are removed by dry and wet deposition processes.

For isoprene SOA, we used the explicit isoprene chemistry developed by Marais et al. (2016). All the isoprene-derived gas-phase products, including isoprene peroxy radical, ISOPOOH, IEPOX, glyoxal, and methylglyoxal, are explicitly simulated. Irreversible heterogeneous uptake of precursors to aqueous aerosols are further calculated using online aerosol pH and surface area.

GEOS-Chem was used to estimate the relative fractions of the measured SOA in our studies between anthropogenic and biogenic (isoprene and monoterpene) sources (Fig. 1). Extensive research has been conducted to evaluate and improve the models performance in predicting BSOA, as summarized in Table S3. Though these evaluations mainly occurred in the southeast US, a recent study has also included more global observations to compare with GEOS-Chem (Pai et al., 2020). Generally, GEOS-Chem appears to overestimate biogenically derived SOA; however, the model predicted SOA is typically within the uncertainty of the AMS

~~(Table S3). The overestimation, though, would suggest that the fraction of urban SOA may be under-predicted by this method, whereas the BSOA may be over-predicted. Therefore, in urban regions, the amount of SOA from biogenic sources may be lower, especially after the rapid SOA enhancements (within 12 to 24 equivalent photochemical hours that have been observed around the world (Nault et al., 2018)). Typically the BSOA is present as a regional background and subtracted for the analyses used in this work, which focus on strong urban plumes on top of that background (Hayes et al., 2013, 2015).~~

~~2.5.2 Default GEOS-Chem Sensitivity to ASOA Simulations~~

~~For the sensitivity calculation using the "traditional" ASOA precursors, we used the two-product model framework (Pye and Seinfeld, 2010). Benzene, toluene, and xylene are oxidized with OH and converted to peroxy radicals. These peroxy radicals react with~~ ~~HO_2~~ ~~or NO, resulting in non-volatile ASOA (~~~~HO_2~~ ~~pathway, ASOAN species in GEOS-Chem) or semi-volatile ASOA tracers (NO pathway, ASOA1-3 in GEOS-Chem). As is the case for monoterpene and sesquiterpene SOA above, GEOS-Chem calculates online partitioning and dry/wet deposition processes for semi-volatile ASOA tracers. Other conditions including mortality calculation are kept the same as the base simulation above.~~

2.3~~6~~ Estimation of Premature Mortality Attribution

Premature deaths were calculated for five disease categories: ischemic heart disease (IHD), stroke, chronic obstructive pulmonary disease (COPD), acute lower respiratory illness

(ALRI), and lung cancer (LC). We calculated premature mortality for the population aged more than 30 years, using Eq. 8~~4~~.

$$Premature\ Death = Pop \times y_0 \times \frac{RR - 1}{RR} \qquad \text{Eq. } 8\cancel{4}$$

Mortality rate, y_0, varies according to the particular disease category and geographic region, which is available from Global Burden of Disease (GBD) Study 2015 database (IHME, 2016). Population (Pop) was obtained from Columbia University Center for International Earth Science Information Network (CIESIN) for 2010 (CIESIN, 2017). Relative risk, RR, can be calculated as shown in Eq. 9~~5~~.

$$RR = 1 + \alpha \times \left(1 - exp\left(\beta \times \left(PM_{2.5} - PM_{2.5,Threshold}\right)^{\rho}\right)\right) \qquad \text{Eq. } 9\cancel{5}$$

α, β, and ρ values depend on disease category and are calculated from Burnett et al. (2014) (see Table S14~~2~~ and associated file). If the $PM_{2.5}$ concentrations are below the $PM_{2.5}$ threshold value (Table S14~~2~~), premature deaths were computed as zero. However, there could be some health impacts at concentrations below the $PM_{2.5}$ threshold values (Krewski et al., 2009); following the methods of the GBD studies, these can be viewed as lower bounds on estimates of premature deaths.

We performed an additional sensitivity analysis using the Global Exposure Mortality Model (GEMM) (Burnett et al., 2018). For the GEMM analysis, we also used age stratified population data from GWPv3. Premature death is calculated the same as shown in Eq. 8~~4~~; however, the relative risk differs. For the GEMM model, the relative risk can be calculated as shown in Eq. 10~~6~~.

$$RR = exp(\theta \times \lambda) \text{ with } \lambda = \frac{\log\left(1+\frac{z}{\alpha}\right)}{\left(1+\exp\left(\frac{(\hat{\mu}-z)}{\pi}\right)\right)}$$

Eq. 10~~6~~

Here z = max(0,$PM_{2.5}$-$PM_{2.5,Threshold}$); θ, π, $\hat{\mu}$, α, and $PM_{2.5,Threshold}$ depends on disease category and are from Burnett et al. (2018). Similar to the Eq. 9~~5~~, if the concentrations are below the threshold (2.4 µg m^{-3}, Burnett et al. (2018)), then premature deaths are computed as zero; however, the GEMM has a lower threshold than the GBD method.

For GBD, we do not consider age-specific mortality rates or risks. For GEMM, we calculate age-specific health impacts with age-specific parameters in the exposure response function (Table S15~~3~~). We combine the age-specific results of the exposure-response function with age distributed population data from GPW (CIESIN, 2017) and a national mortality rate across all ages to assess age-specific mortality.

We calculated total premature deaths using annual average total $PM_{2.5}$ concentrations derived from satellite-based estimates at the resolution of 0.1°×0.1° from van Donkelaar et al. (2016) . Application of the remote-sensing based $PM_{2.5}$ at the 0.1°×0.1° resolution rather than direct use of the GEOS-Chem model concentrations at the 2°×2.5° resolution helps reduce uncertainties in the quantification of $PM_{2.5}$ exposure inherent in coarser estimates (Punger and West, 2013). We also calculated deaths by subtracting from this amount the total annual average ASOA concentrations derived from GEOS-Chem (Fig. S11~~9~~). To reduce uncertainties related to spatial gradients and total concentration magnitudes in our GEOS-Chem simulations of $PM_{2.5}$, our modeled ASOA was calculated as the fraction of ASOA to total $PM_{2.5}$ in GEOS-Chem, multiplied by the satellite-based PM2.5 concentrations (Eq. 11~~7~~).

$$ASOA_{sat} = (ASOA_{mod}/PM_{2.5,mod}) \times PM_{2.5,sat}$$

Eq. 11~~7~~

Finally, this process for estimating $PM_{2.5}$ health impacts considers only $PM_{2.5}$ mass concentration and does not distinguish toxicity by composition, consistent with the current US EPA position expressed in Sacks et al. (2019).

3. Observations of ASOA Production across Three Continents

3.1 Observational Constraints of ASOA Production across Three Continents

Measurements during intensive field campaigns in large urban areas better constrain concentrations and atmospheric formation of ASOA because the scale of ASOA enhancement is large compared to SOA from a regional~~from regional~~ background. Generally, ASOA increased with the amount of urban precursor VOCs and with atmospheric PA (de Gouw et al., 2005; de Gouw and Jimenez, 2009; DeCarlo et al., 2010; Hayes et al., 2013; Nault et al., 2018; Schroder et al., 2018; Shah et al., 2018). In addition, ASOA correlates strongly with gas-phase secondary photochemical species, including O_x, HCHO, and PAN (Herndon et al., 2008; Wood et al., 2010; Hayes et al., 2013; Zhang et al., 2015; Nault et al., 2018; Liao et al., 2019) (Table S4; Fig. S1~~2~~ to Fig. S3~~4~~), which are indicators of photochemical processing of emissions.

However, as initially discussed by Nault et al. (2018) and shown in Fig. 3~~4,~~ there is large variability in these various metrics across the urban areas evaluated here. To the best of the authors' knowledge, this variability has not been explored and its physical meaning has not been interpreted. As shown in Fig. 3~~4~~, though, the trends in ΔSOA/ΔCO are similar to the trends in the slopes of SOA versus O_x, PAN, or HCHO. For example, Seoul is the highest for nearly all metrics, and is approximately a factor of 6 higher than the urban area, Houston, that generally showed the lowest photochemical metrics. This suggests that the variability is related to a physical factor, including emissions and chemistry.

The VOC concentration, together with how quickly the emitted VOCs react ($\Sigma k_i \times [VOC]_i$, i.e., the hydroxyl radical, or OH, reactivity of VOCs), where k is the OH rate coefficient for each VOC, are a determining parameter for ASOA formation over urban spatial scales (Eq. 12~~8~~). ASOA formation is normalized here to the excess CO mixing ratio (ΔCO) to account for the effects of meteorology, dilution, and non-urban background levels, and allow for easier comparison between different studies:

$$\frac{\Delta \mathrm{ASOA}}{\Delta \mathrm{CO}} \propto [\mathrm{OH}] \times \Delta t \times \left(\sum_i k_i \times \left[\frac{\mathrm{VOC}}{\mathrm{CO}} \right]_i \times \mathrm{Y_i} \right)$$

Eq. 12~~8~~

where Y is the aerosol yield for each compound (mass of SOA formed per unit mass of precursor reacted), and $[OH] \times \Delta t$ is the PA.

BTEX are one group of known ASOA precursors (Gentner et al., 2012; Hayes et al., 2013), and their emission ratio (to CO) was determined for all campaigns (Table S5). BTEX can thus provide insight into ASOA production. Fig. 2~~5~~a shows that the variation in ASOA (at PA = 0.5 equivalent days) is highly correlated with the emission reactivity ratio of BTEX (R_{BTEX}, $\Sigma_i [\mathrm{VOC}/\mathrm{CO}]_i$) across all the studies. However, BTEX alone cannot account for much of the ASOA formation (see budget closure discussion below), and instead, BTEX may be better thought of as both partial contributors and also as indicators for the co-emission of other (unmeasured) organic precursors that are also efficient at forming ASOA.

O_x, PAN, and HCHO are produced from the oxidation of a much wider set of VOC precursors (including small alkenes, which do not appreciably produce SOA when oxidized). These alkenes have similar reaction rate constants with OH as the most reactive BTEX compounds (Table S12~~1~~); however, their emissions and concentration can be higher than BTEX (Table S7). Thus, alkenes would dominate R_{Total}, leading to O_x, HCHO, and PAN being produced more rapidly than ASOA (Fig. 2~~5~~b–d). When R_{BTEX} becomes more important for R_{Total}, the emitted VOCs are more efficient in producing ASOA. Thus, the ratio of ASOA to gas-phase photochemical products shows a strong correlation with R_{BTEX}/R_{Total} (Fig. 2~~5~~b–d).

An important aspect of this study is that most of these observations occurred during spring and summer, when solid fuel emissions are expected to be lower (e.g., Chafe et al., 2015; Lam et al., 2017; Hu et al., 2020). Further, the most important observations used here are during the afternoon, investigating specifically the photochemically produced ASOA. These results here might partially miss any ASOA produced through nighttime aqueous chemistry or oxidation by nitrate radical (Kodros et al., 2020). However, two of the studies included in our analysis, Chinese Outflow (CAPTAIN, 2011) and New York City (WINTER, 2015), occurred in late winter/early spring, when solid fuel emissions were important (Hu et al., 2013; Schroder et al., 2018). We find that these observations lie within the uncertainty in the slope between ASOA and R_{BTEX} (Fig. 2a). Their photochemically produced ASOA observed under strong impact from solid fuel emissions shows similar behavior as the ASOA observed during spring and summer time. Thus, given the limited datasets currently available, photochemically produced ASOA is expected to follow the relationship shown in Fig. 2a and is expected to also follow this relationship for regions impacted by solid fuel burning. Future comprehensive studies in regions strongly impacted by solid fuel burning are needed to further investigate photochemical ASOA production under those conditions.

3.2 Budget Closure of ASOA for 4 Urban Areas on 3 Continents Indicates Reasonable Understanding of ASOA Sources

To investigate the correlation between ASOA and R_{BTEX}, a box model using the emission ratios from BTEX (Table S5), other aromatics (Table S8), IVOCs (Sect. S1), and SVOCs (Sect. S1) was run for five urban areas: New York City, 2002, Los Angeles, Beijing, London, and New York City, 2015 (see Sect. S1 and S3 for more information). The differences in the results shown in Fig. 4 are due to differences in the emissions for each city. We show that BTEX alone cannot explain the observed ASOA budget for urban areas around the world. Fig. 4~~6~~a shows that approximately 25±6% of the observed ASOA originates from the photooxidation of BTEX. ~~Therefore, other precursors must account for most of the ASOA produced.~~ BTEX only explaining 25% of the observed ASOA is similar to prior studies that have done budget analysis of precursor gases and observed SOA (e.g., Dzepina et al., 2009; Ensberg et al., 2014; Hayes et al., 2015; Ma et al., 2017; Nault et al., 2018). Therefore, other precursors must account for most of the ASOA produced.

Because alkanes, alkenes, and oxygenated compounds with carbon numbers less than 6 are not significant ASOA precursors, we focus on emissions and sources of BTEX, other mono-aromatics, IVOCs, and SVOCs. These three classes of VOCs, aromatics, IVOCs, and SVOCs, have been suggested to be significant ASOA precursors in urban atmospheres (Robinson et al., 2007; Hayes et al., 2015; Ma et al., 2017; McDonald et al., 2018; Nault et al., 2018; Schroder et al., 2018; Shah et al., 2018), originating from both fossil fuel and VCP emissions.

Using the best available emission inventories from cities on three continents (EMEP/EEA, 2016; McDonald et al., 2018; Li et al., 2019) and observations, we quantify the emissions of BTEX, other mono-aromatics, IVOCs, and SVOCs for both fossil fuel (e.g., gasoline, diesel, kerosene, etc.), VCPs (e.g., coatings, inks, adhesives, personal care products, and cleaning agents), and cooking sources (Fig. 5~~2 and Fig. 3~~). This builds off the work of McDonald et al. (2018) for urban regions on three different continents.

Note, the emissions investigated here ignore any oxygenated VOC emissions not associated with IVOCs and SVOCs due to the challenge in estimating the emission ratios for these compounds (de Gouw et al. 2018). Further, SVOC emission ratios are estimated from the average POA observed by the AMS during the specific campaign and scaled by profiles in literature for a given average temperature and average OA (Robinson et al., 2007; Worton et al., 2014; Lu et al., 2018). As most of the campaigns had an average OA between 1 and 10 μg m^{-3} and temperature of ~298 K, this led to the majority of the estimated emitted SVOC gases in the highest SVOC bin. However, as discussed later, this does not lead to SVOCs dominating the predicted ASOA due to taking into account the fragmentation and overall yield from the photooxidation of SVOC to ASOA.

Combining these inventories and observations for the various locations provide the following insights about the potential ASOA precursors not easily measured or quantified in urban environments (e.g., Zhao et al., 2014; Lu et al., 2018): (1) aromatics from fossil fuel accounts for 14-40% (mean 22%) of the total BTEX and IVOC emissions for the five urban areas investigated in-depth (Fig. 5~~2~~), agreeing with prior studies that have shown that the observed ASOA cannot be reconciled by the observations or emission inventory of aromatics from fossil fuels (e.g., Ensberg et al., 2014; Hayes et al., 2015). (2) BTEX from both fossil fuels and VCPs account for 25-95% (mean 43%) of BTEX and IVOC emissions (Fig. 5~~2~~). China has the lowest contribution of IVOCs, potentially due to differences in chemical make-up of the solvents used daily (Li et al., 2019), but more research is needed to investigate the differences in IVOCs:BTEX from Beijing versus US and UK emission inventories. Nonetheless, this shows the importance of IVOCs for both emissions and ASOA precursors. (3) IVOCs are generally equal to, if not greater than, the emissions of BTEX in 4 of the 5 urban areas investigated here (Fig. 5~~2~~). (4) Overall, VCPs account for a large fraction of the BTEX and IVOC emissions for all five cities. (5) Finally, SVOCs account for 27-88% (mean 53%) of VOCs generally considered ASOA precursors (VOCs with volatility saturation concentrations ≤ 10^{7} μg m^{-3}) (Fig. S6~~3~~). Beijing has the highest contribution of SVOCs to ASOA precursors due to the use of solid fuels and cooking emissions (Hu et al., 2016). Also, this indicates the large contribution of a class of VOCs difficult to measure (Robinson et al., 2007) that are an important ASOA precursor (e.g., Hayes et al., 2015), showing further emphasis should be placed in quantifying the emissions of this class of compounds.

These results provide an ability to further investigate the mass balance of predicted and observed ASOA for these urban locations (Fig. 4~~6~~). The inclusion of IVOCs, other aromatics not including BTEX, and SVOCs leads to the ability to explain, on average, 85±12% of the observed ASOA for these urban locations around the world (Fig. 4~~6~~a). Further, VCP contribution to

ASOA is important for all these urban locations, accounting for~~accounting or~~, on average, 37±3% of the observed ASOA (Fig. 4~~6~~b).

This bottom-up mass budget analysis provides important insights to further explain the correlation observed in Fig. 2~~5~~. First, IVOCs are generally co-emitted from similar sources as BTEX for the urban areas investigated in-depth (Fig. 5~~2~~). The oxidation of these co-emitted species leads to the ASOA production observed across the urban areas around the world. Second, S/IVOCs generally have similar rate constants as toluene and xylenes ($\geq 1\times10^{-11}$ cm^3 molec.$^{-1}$ s^{-1}) (Zhao et al., 2014, 2017), the compounds that contribute the most to R_{BTEX}, explaining the rapid ASOA production that has been observed in various studies (de Gouw and Jimenez, 2009; DeCarlo et al., 2010; Hayes et al., 2013; Hu et al., 2013, 2016; Nault et al., 2018; Schroder et al., 2018) and correlation (Fig. 2~~5~~). Finally, the contribution of VCPs and fossil fuel sources to ASOA is similar across the cities, expanding upon and further supporting the conclusion of McDonald et al. (2018) in the importance of identifying and understanding VCP emissions in order to explain ASOA.

This investigation shows that the bottom-up calculated ASOA agrees with observed top-down ASOA within 15%. As highlighted above, this ratio is explained by the co-emissions of IVOCs with BTEX from traditional sources (diesel, gasoline, and other fossil fuel emissions) and VCPs (Fig. 5) along with similar rate constants for these ASOA precursors (Table S12). Thus, the ASOA/R_{BTEX} ratio obtained from Fig. 2 results in accurate predictions of ASOA for the urban areas evaluated here, and this value can be used to better estimate ASOA with chemical transport models (Sect. 4).

4. Improved Urban SIMPLE Model Using Multi-Cities to Constrain

~~4.1 Updates to the SIMPLE Model~~

~~With the combination of the new dataset, which expands across urban areas on three continents, the SIMPLE parameterization for ASOA (Hodzic and Jimenez, 2011) is updated in the standard GEOS-Chem model to reproduce observed ASOA in Fig. 5a. The parameterization operates as represented by Eq. 9.~~

$$\text{Emissions} \rightarrow \text{SOAP} \xrightarrow{k \times [\text{OH}]} \text{ASOA}$$ ~~Eq. 9~~

~~SOAP represents the lumped precursors of ASOA, k is the reaction rate coefficient with OH (1.25×10^{-11} cm^3 molecules^{-1} s^{-1}), and [OH] is the OH concentration in molecules cm^{-3}.~~

~~SOAP emissions were calculated based on the relationship between ΔSOA/ΔCO and $R_{aromatics}$/ΔCO in Fig. 5a. First, we calculated $R_{aromatics}$/ΔCO (Eq. 10) for each grid cell and time step as follows:~~

$$\frac{R_{\text{aromatics}}}{\Delta \text{CO}} = \frac{E_B \times k_B + E_T \times k_T + E_X \times k_X}{E_{CO}}$$ ~~Eq. 10~~

~~Where E and k stand for the emission rate and reaction rate coefficient with OH, respectively, for benzene (B), toluene (T), and xylenes (X). Ethylbenzene was not included in this calculation because its emission was not available in HTAPv2 emission inventory. However, ethylbenzene contributed a minor fraction of the mixing ratio (~ 7%, Table S5) and reactivity (~6%) of the total BTEX across the campaigns. Reaction rate constants used in this study were 1.22×10^{-12}, 5.63×10^{-12}, and 1.72×10^{-11} cm^3 molec.$^{-1}$ s^{-1} for benzene, toluene, and xylene, respectively (Atkinson and Arey, 2003; Atkinson et al., 2006).~~

~~Second, E_{SOAP}/E_{CO} can be obtained from the result of Eq. 11, using slope and intercept in Fig. 5a, with a correction factor (F) to consider additional SOA production after 0.5 PA equivalent days, since Fig. 5a shows the comparison at 0.5 PA equivalent days.~~

$$\frac{E_{SOAP}}{E_{CO}} = \left(Slope \times \frac{R_{Aromatics}}{\Delta CO} + Intercept \right) \times F \qquad \text{~~Eq. 11~~}$$

~~Where slope is 24.8 and intercept is –1.7 from Fig. 5a. F (Eq. 12) can be calculated as follows:~~

$$F = \frac{ASOA_{t=\infty}}{ASOA_{t=0.5d}} = \frac{SOAP_{t=0}}{SOAP_{t=0} \times (1 - exp(-k \times \Delta t \times [OH]))}, \Delta t = 43200\ s \qquad \text{~~Eq. 12~~}$$

~~F was calculated as 1.8 by using [OH] = 1.5 × 10^6 molecules cm^{-3}, which was used in the definition of 0.5 PA equivalent days for Fig. 5a.~~

~~Finally, E_{SOAP} can be computed by multiplying CO emissions (E_{CO}) for every grid point and time step in GEOS-Chem by the E_{SOAP}/E_{CO} ratio.~~

~~4.2 Results of Updated SIMPLE Model~~

The SIMPLE model was originally designed and tested against the observations collected around Mexico City (Hodzic and Jimenez, 2011). It was then tested against observations collected in Los Angeles (Hayes et al., 2015; Ma et al., 2017). As both data sets have nearly identical ΔSOA/ΔCO and R_{BTEX} (Fig. 2~~4~~ and Fig. 3~~5~~), it is not surprising that the SIMPLE model did well in predicting the observed ΔSOA/ΔCO for these two urban regions with consistent parameters. Though the SIMPLE model generally performed better than more explicit models, it generally had lower skill in predicting the observed ASOA in urban regions outside of Mexico City and Los Angeles (Shah et al., 2019; Pai et al., 2020).

This may stem from the original SIMPLE model with constant parameters missing the ability to change the amount and reactivity of the emissions, which are different for the various urban regions, versus the ASOA precursors being emitted proportionally to only CO (Hodzic and Jimenez, 2011; Hayes et al., 2015). For example, in the HTAP emissions inventory, the CO emissions for Seoul, Los Angeles, and Mexico City are all similar (Fig. S8); thus, the original SIMPLE model would suggest similar ΔSOA/ΔCO for all three urban locations. However, as shown in Fig. 2~~4~~ and Fig. 3~~5~~, the ΔSOA/ΔCO is different by nearly a factor of 2. The inclusion of the emissions and reactivity, where R_{BTEX} for Seoul is approximately a factor of 2.5 higher than Los Angeles and Seoul, into the improved SIMPLE model better accounts for the variability in SOA production, as shown in Fig. 2~~5~~. Thus, the inclusion and use of this improved SIMPLE model refines the simplified representation of ASOA in chemical transport models and/or box models.

The "improved" SIMPLE shows higher ASOA compared to the default VBS GEOS-Chem (Fig. 6a,b). In areas strongly impacted by urban emissions (e.g., Europe, East Asia, India, east and west coast US, and regions impacted by Santiago, Chile, Buenos Aires, Argentina, Sao Paulo, Brazil, Durban and Cape Town, South Africa, and Melbourne and Sydney, Australia), the "improved" SIMPLE model predicts up to 14 μg m^{-3} more ASOA, or ~30 to 60 times more ASOA than the default scheme (Fig. 6c,d). As shown in Fig. 1, during intensive measurements, the ASOA composed 17-39% of PM_1, with an average contribution of ~25%. The default ASOA scheme in GEOS-Chem greatly underestimates the fractional contribution of ASOA to total $PM_{2.5}$ (<2%; Fig. 6e). The "improved" SIMPLE model greatly improves the predicted fractional contribution, showing that ASOA in the urban regions ranges from 15-30%, with an average of ~15% for the grid cells corresponding to the urban areas investigated here (Fig. 6f). Thus, the "improved" SIMPLE predicts the fractional contribution of ASOA to total $PM_{2.5}$ far more realistically, compared to observations. As discussed in Sect. 2.3 and Eq. 11, having the model accurately predict the fractional contribution of ASOA to the total PM is very important, as the total $PM_{2.5}$ is derived from satellite-based estimates (van Donkelaar et al., 2015), and the model fractions are then applied to those total $PM_{2.5}$ estimates. The ability for the "improved" SIMPLE model to better represent the ASOA composition provides confidence attributing the ASOA contribution to premature mortality.

5. Preliminary Evaluation of Worldwide Premature Deaths Due to ASOA with Updated SIMPLE Parameterization

The improved SIMPLE parameterization is used along with GEOS-Chem to provide an accurate estimation of ASOA formation in urban areas worldwide and provide an ability to obtain realistic simulations of ASOA based on measurement data. We use this model to quantify the attribution of $PM_{2.5}$ ASOA to premature deaths. Analysis up to this point has been for PM_1; however, both the chemical transport model and epidemiological studies utilize $PM_{2.5}$. For ASOA, this will not impact the discussion and results here because the mass of OA (typically 80–90%) is dominated by PM_1 (e.g., Bae et al., 2006; Seinfeld and Pandis, 2006), and ASOA is formed mostly through condensation of oxidized species, which favors partitioning onto smaller particles (Seinfeld and Pandis, 2006).

The procedure for this analysis is described in Fig. 7 and Sect. 2.3~~5~~ and S3~~2.6~~. Briefly, we combine high-resolution satellite-based $PM_{2.5}$ estimates (for exposure) and a chemical transport model (GEOS-Chem, for fractional composition) to estimate ASOA concentrations and various sensitivity analysis (van Donkelaar et al., 2015). We calculated ~3.3 million premature deaths (using the Integrated Exposure-Response, IER, function) are due to long-term exposure of ambient $PM_{2.5}$ (Fig. S9~~7~~, Table S16~~4~~), consistent with recent literature (Cohen et al., 2017).

The attribution of ASOA $PM_{2.5}$ premature deaths can be calculated one of two ways: (a) marginal method (Silva et al., 2016) or (b) attributable fraction method (Anenberg et al., 2019). For method (a), it is assumed that a fraction of the ASOA is removed, keeping the rest of the $PM_{2.5}$ components approximately constant, and the change in deaths is calculated from the deaths associated with the total concentration less the deaths calculated using the reduced total $PM_{2.5}$ concentrations. For method (b), the health impact is attributed to each $PM_{2.5}$ component by multiplying the total deaths by the fractional contribution of each component to total $PM_{2.5}$. For method (a), the deaths attributed to ASOA are ~340,000 people per year (Fig. 8); whereas, for method (b), the deaths are ~370,000 people per year. Both of these are based on the IER response function (Cohen et al., 2017).

Additional recent work (Burnett et al., 2018) has suggested less reduction in the premature deaths versus $PM_{2.5}$ concentration relationship at higher $PM_{2.5}$ concentrations, and lower concentration limits for the threshold below which this relationship is negligible, both of which lead to much higher estimates of $PM_{2.5}$ associated premature deaths. This is generally termed the Global Exposure Mortality Model (GEMM). Using the two attribution methods described above (a and b), the ASOA $PM_{2.5}$ premature deaths are estimated to be ~640,000 (method a) and ~900,000 (method b) (Fig. S9~~7~~ and Fig. S12~~0~~ and Table S17~~5~~).

Compared to prior studies using chemical transport models to estimate premature deaths associated with ASOA (e.g., Silva et al., 2016; Ridley et al., 2018), which assumed non-volatile POA and "traditional" ASOA precursors, the attribution of premature mortality due to ASOA is over an order of magnitude higher in this study (Fig. 9). This occurs using either the IER and GEMM approach for estimating premature mortality (Fig. 9). For regions with larger populations and more $PM_{2.5}$ pollution, the attribution is between a factor of 40 to 80 higher. This stems from the non-volatile POA and "traditional" ASOA precursors over-estimating POA and under-estimating ASOA compared to observations (Schroder et al., 2018). These offsetting errors will lead to model predicted total OA similar to observations (Ridley et al., 2018; Schroder et al., 2018), yet different conclusions on whether POA versus SOA is more important for reducing $PM_{2.5}$ associated premature mortality. Using a model constrained to day-time atmospheric observations (Fig. 2~~5~~ and Fig. 4~~6~~, see Sect. 4) leads to a more accurate estimation of the contribution of photochemically-produced ASOA to $PM_{2.5}$ associated premature mortality that has not been possible in prior studies. We note that ozone concentrations change little as we change the ASOA simulation (see Sect. S4~~ in the SI~~ and Fig. S14~~2~~).

A limitation in this study is the lack of sufficient measurements in South and Southeast Asia, Eastern Europe, Africa, and South America (Fig. 1), though these areas account for 44% of the predicted reduction in premature mortality for the world (Table S16~~4~~). However, as highlighted in Table S18~~6~~, these regions likely still consume both transportation fuels and VCPs, although in lower per capita amounts than more industrialized countries. This consumption is expected to lead to the same types of emissions as for the cities studied here, though more field measurements are needed to validate global inventories of VOCs and resulting oxidation products in the developing world. Transportation emissions of VOCs are expected to be more dominant in the developing world due to higher VOC emission factors associated with inefficient combustion engines, such as two-stroke scooters (Platt et al., 2014) and auto-rickshaws (e.g., Goel and Guttikunda, 2015).

Solid fuels are used for residential heating and cooking, which impact the outdoor air quality as well (Hu et al., 2013, 2016; Lacey et al., 2017; Stewart et al., 2020), and which also lead to SOA (Heringa et al., 2011). As discussed in Sect. 3.1, though the majority of the studies evaluated here occurred in spring to summer time, when solid fuel emissions are decreased, two studies occurred during the winter/early spring time, where solid fuel emissions were important (Hu et al., 2013; Schroder et al., 2018). These studies still follow the same relationship between ASOA and R_{BTEX} as the studies that focused on spring/summer time photochemistry. Thus, the limited datasets available indicate that photochemically produced ASOA from solid fuels follow a similar relationship to that from other ASOA sources.

Also, solid fuel sources are included in the inventories used in our modeling. For the HTaP emission inventory used here (Janssens-Maenhout et al., 2015), small-scale combustion, which includes heating and cooking (e.g., solid-fuel use), is included in the residential emission sector. Both CO and BTEX are included in this source, and can account for a large fraction of the total emissions where solid-fuel use may be important (Fig. S15). Thus, as CO and BTEX are used in the updated SIMPLE model, and campaigns that observed solid-fuel emissions fall within the trend for all urban areas, the solid-fuel contribution to photochemically-produced ASOA is accounted for (as accurately as allowed by current datasets) in the estimation of ASOA for the attribution to premature mortality.

Note that recent work has observed potential nighttime aqueous chemistry and/or oxidation by nitrate radical from solid fuel emissions to produce ASOA (Kodros et al., 2020). Thus, missing this source of ASOA may lead to an underestimation of total ASOA versus the photochemically-produced ASOA we discuss here, leading to a potential underestimation in the attribution of ASOA to premature mortality. From the studies that investigated "night-time aging" of solid-fuel emissions to form SOA, we predict that the total ASOA may be underestimated by 1 to 3 μg m^{-3} (Kodros et al., 2020). This potential underestimation, though, is less than the current underestimation in ASOA in GEOS-Chem (default versus "Updated" SIMPLE).

~~Also, unlike many of the cities studied here, solid fuels are used for residential heating and cooking, which impact the outdoor air quality as well (Hu et al., 2013, 2016; Lacey et al., 2017; Stewart et al., 2020), and which also lead to SOA (Heringa et al., 2011).~~ Recently, emission factors from Abidjan, Côte d'Ivoire, a developing urban area, showed the dominance of emissions from transportation and solid fuel burning, with BTEX being an important fraction of the total emissions, and that all the emissions were efficient in producing ASOA (Dominutti et al., 2019). Further, investigation of emissions in New Delhi region of India demonstrated the importance of both transportation and solid fuel emissions (Stewart et al., 2020; Wang et al., 2020) while model comparisons with observations show an underestimation of OA compared to observations due to a combination of emissions and OA representation (Jena et al., 2020). Despite emission source differences, SOA is still an important component of $PM_{2.5}$ (e.g., Singh et al., 2019) and thus will impact air quality and premature mortality in developing regions. Admittedly, though, our estimates will be less accurate for these regions.

6. Conclusions

In summary, ASOA is an important, though inadequately constrained component of air pollution in megacities and urban areas around the world. This stems from the complexity associated with the numerous precursor emission sources, chemical reactions, and oxidation products that lead to observed ASOA concentrations. We have shown here that the variability in observed ASOA across urban areas is correlated with R_{BTEX}, a marker for the co-emissions of IVOC from both transportation and VCP emissions. Global simulations indicate ASOA contributes to a substantial fraction of the premature mortality associated with $PM_{2.5}$. Reductions of the ASOA precursors will reduce the premature deaths associated with $PM_{2.5}$, indicating the importance of identifying and reducing exposure to sources of ASOA. These sources include emissions that are both traditional (transportation) as well as non-traditional emissions of emerging importance (VCPs) to ambient $PM_{2.5}$ concentrations in cities around the world. Further investigation of speciated IVOCs and SVOCs for urban areas around the world along with SOA mass concentration and other photochemical products (e.g., O_x, PAN, and HCHO) for other urban areas, especially in South Asia, throughout Africa, and throughout South America, would provide further constraints to improve the SIMPLE model and our understanding of the emission sources and chemistry that leads to the observed SOA and its impact on premature mortality.

Acknowledgements

This study was partially supported by grants from NASA NNX15AT96G, NNX16AQ26G, Sloan Foundation 2016-7173, NSF AGS-1822664, EPA STAR 83587701-0, NERC NE/H003510/1, NERC NE/H003177/1, NERC NE/H003223/1, NOAA NA17OAR4320101, NCAS R8/H12/83/037, Natural Science and Engineering Research Council of Canada (NSERC, RGPIN/05002-2014), and the Fonds de Recherche du Québec —Nature et technologies (FRQNT, 2016-PR-192364). This manuscript has not been formally reviewed by EPA. The views expressed in this document are solely those of the authors and do not necessarily reflect those of the Agency. EPA does not endorse any products or commercial services mentioned in this publication. We thank Katherine Travis for useful discussions. We acknowledge B J. Bandy, J. Lee, G. P. Mills, d. D. Montzka, J. Stutz, A. J. Weinheimer E. J. Williams, E. C. Wood, and D. R. Worsnop for use of their data.

Data Availability

TexAQS measurements are available at https://esrl.noaa.gov/csl/groups/csl7/measurements/2000TexAQS/LaPorte/DataDownload/ and upon request. NEAQS measurements are available at https://www.esrl.noaa.gov/csl/groups/csl7/measurements/2002NEAQS/. MILAGRO measurements are available at http://doi.org/10.5067/Aircraft/INTEXB/Aerosol-TraceGas. CalNex measurements are available at https://esrl.noaa.gov/csl/groups/csl7/measurements/2010calnex/Ground/DataDownload/. ClearfLo measurements are available at https://catalogue.ceda.ac.uk/uuid/6a5f9eedd68f43348692b3bace3eba45. SEAC^{4}RS measurements are available at http://doi.org/10.5067/Aircraft/SEAC4RS/Aerosol-TraceGas-Cloud. WINTER measurements are available at https://data.eol.ucar.edu/master_lists/generated/winter/. KORUS-AQ measurements are available at http://doi.org/10.5067/Suborbital/KORUSAQ/DATA01. Data from Chinese campaigns are available upon request, and rest of data used were located in papers cited. GEOS-Chem data available upon request. Figures will become accessible at cires1.colorado.edu/jimenez/group_pubs.html.

Competing Interests

The authors declare no competing interests.

Author Contribution

B.A.N., D.S.J., B.C.M., J.A.dG., and J.L.J designed the experiment and wrote the paper. B.A.N., PC.-J., D.A.D., W.H., J.C.S, J.A., D.R.B., M.R.C., H.C., M.M.C., P.F.D, G.S.D., R.D., F.F, A.F., J.B.G., G.G., J.F.H, T.F.H., P.L.H., J.H., M.H., L.G.H., B.T.J., W.C.K., J.L., I.B.P., J.P., B.R.,

C.E.R., D.R., J.M.R., T.B.R, M.S., J.W., C.W., P.W., G.M.W., D.E.Y., B.Y., J.A.dG., and J.L.J. collected and analyzed the data. D.S.J. and A.H. ran the GEOS-Chem model and B.A.N., D.S.J, and J.L.J. analyzed the model output. B.A.N., P.L.H., J.M.S., and J.L.J. ran and analyzed the 0-D model used for ASOA budget analysis of ambient observations. B.C.M., A.L., M.L., and Q.Z. analyzed and provided the emission inventories used for the 0-D box model. D.S.J., D.K.H., and M.O.N. conducted the ASOA attribution to mortality calculation, and B.A.N., D.S.J., D.K.H., M.O.N., J.A.dG, and J.L.J analyzed the results. All authors reviewed the paper.

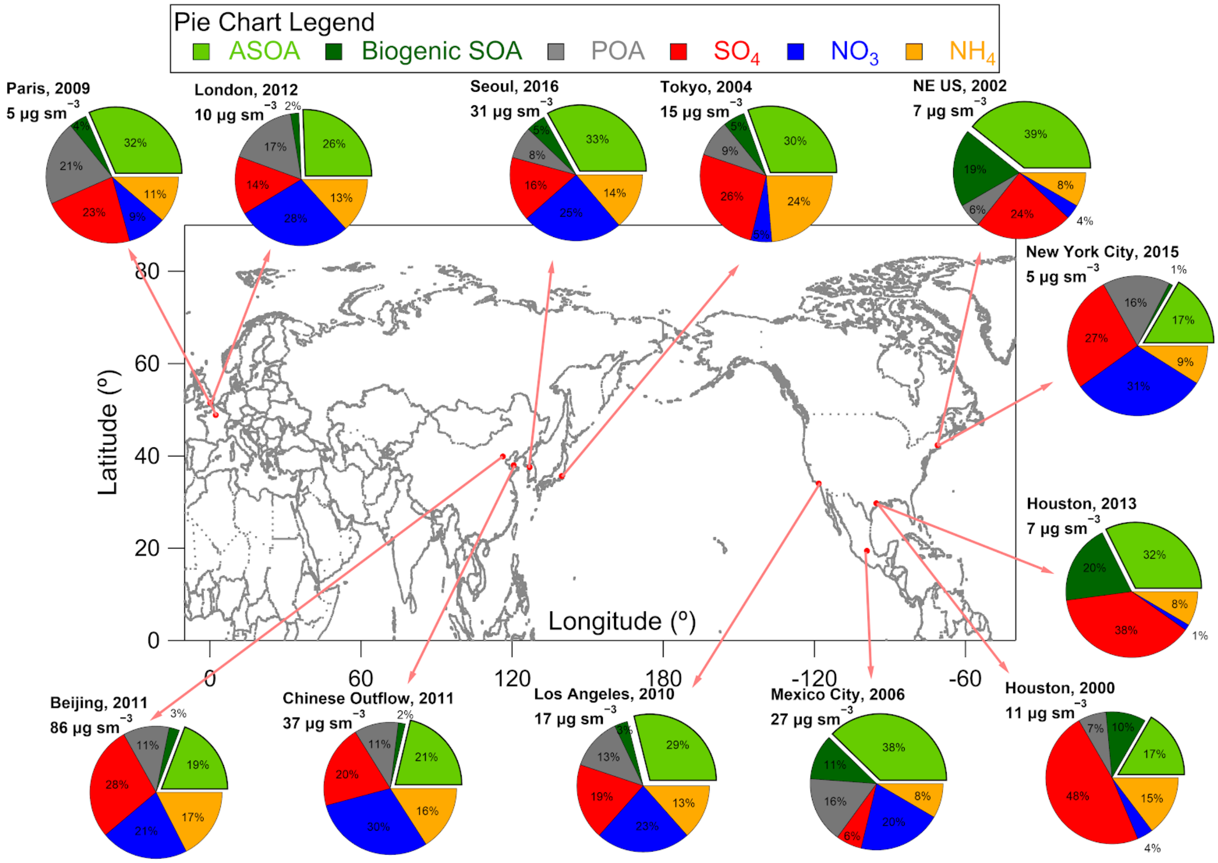

Figure 1. Non-refractory submicron aerosol composition measured in urban and urban outflow regions from field campaigns used in this study, all in units of µg m^{-3}, at standard temperature (273 K) and pressure (1013 hPa) (sm^{-3}). See Sect. S3~~2~~ and ~~(GEOS-Chem Section and~~ Table 1~~)~~ for further information on measurements, studies, and apportionment of SOA into ASOA and BSOA.

~~**Figure 2**. Comparison of BTEX and IVOC sources for (a) Beijing (see SI section about Beijing emission inventory), (b) London (see SI section about London/UK emission inventory), and (c) Los Angeles, (d) Northeast United States, and (e) New York City (see SI section about United States for (c) – (e)). For (a), BTEX is on the left axis and IVOC is on the right axis, due to the small emissions per day for IVOC.~~

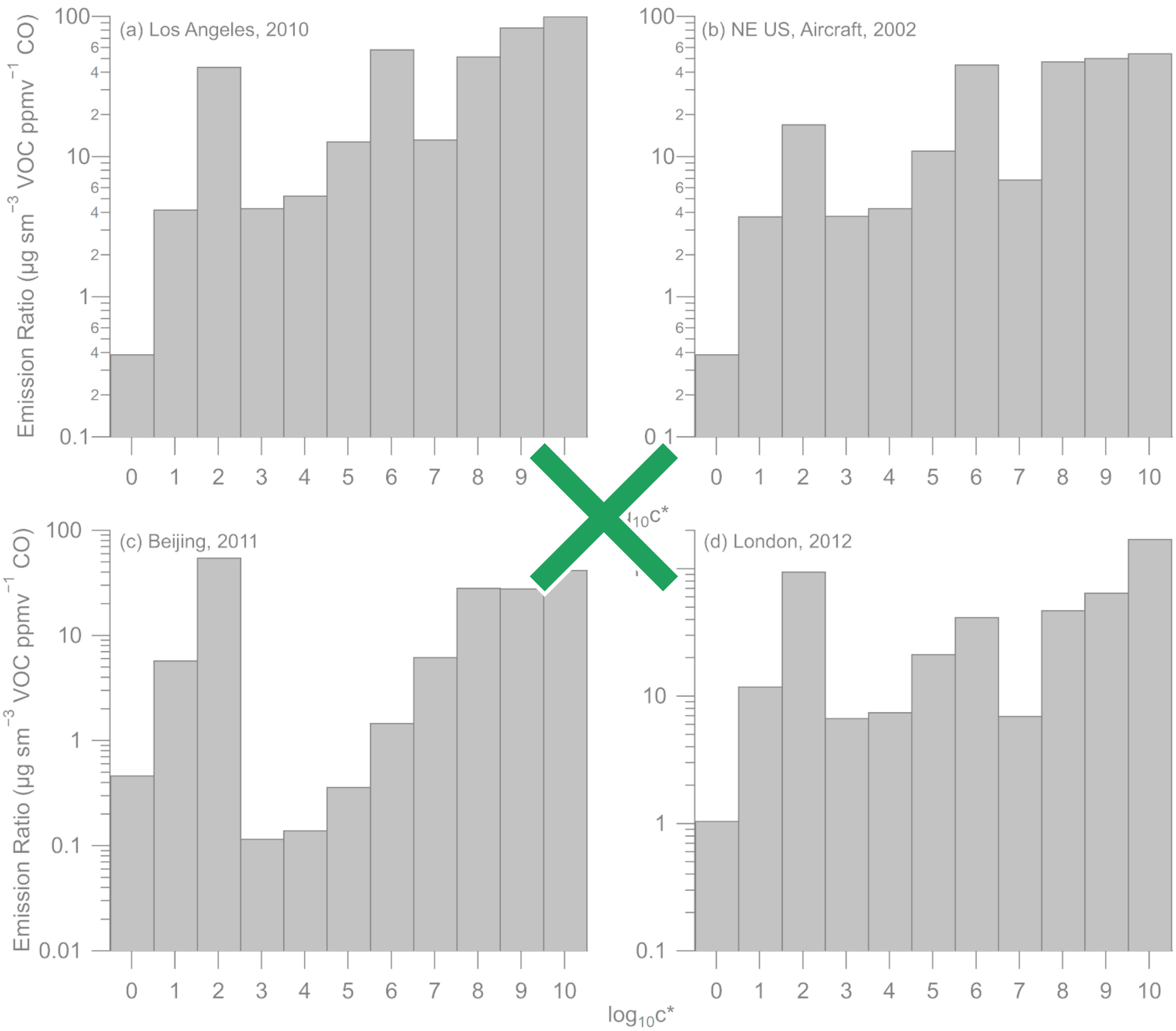

~~**Figure 3**. Emission ratio versus saturation concentration ($\log_{10}(c^*)$) for (a) Los Angeles, (b) NE US, aircraft, (c) Beijing, and (d) London. The emission ratios for VOCs ($\log_{10}(c^*) \geq 7$) were taken from de Gouw et al. (2017) and Ma et al. (2017) for Los Angeles, Warneke et al. (2007) for NE US, aircraft, and Wang et al. (2014) for Beijing while the VOC emission ratio for London is from Table S6 to Table S8. For VOCs between $\log_{10}(c^*)$ of 3 and 6 (IVOCs), the volatility distribution from McDonald et al. (2018), along with the ratio of IVOC to BTEX from Figure SI-6 and the emission ratio of BTEX (Table S6), were used to determine the emission ratio versus saturation concentration. Finally, for VOCs between $\log_{10}(c^*)$ 0 and 2 (SVOCs), the volatility distributions from Robinson et al. (2007) for non-fossil fuel POA and from Worton et al. (2014) for fossil fuel POA were used to convert the normalized POA mass concentration (Table S9) to VOC emission ratios. Note, the emission ratio versus saturation concentration for New York City, 2015, was similar to (b), as the emissions were similar (Fig. 2) and the BTEX for New York City is the same as NE US (Table S5).~~

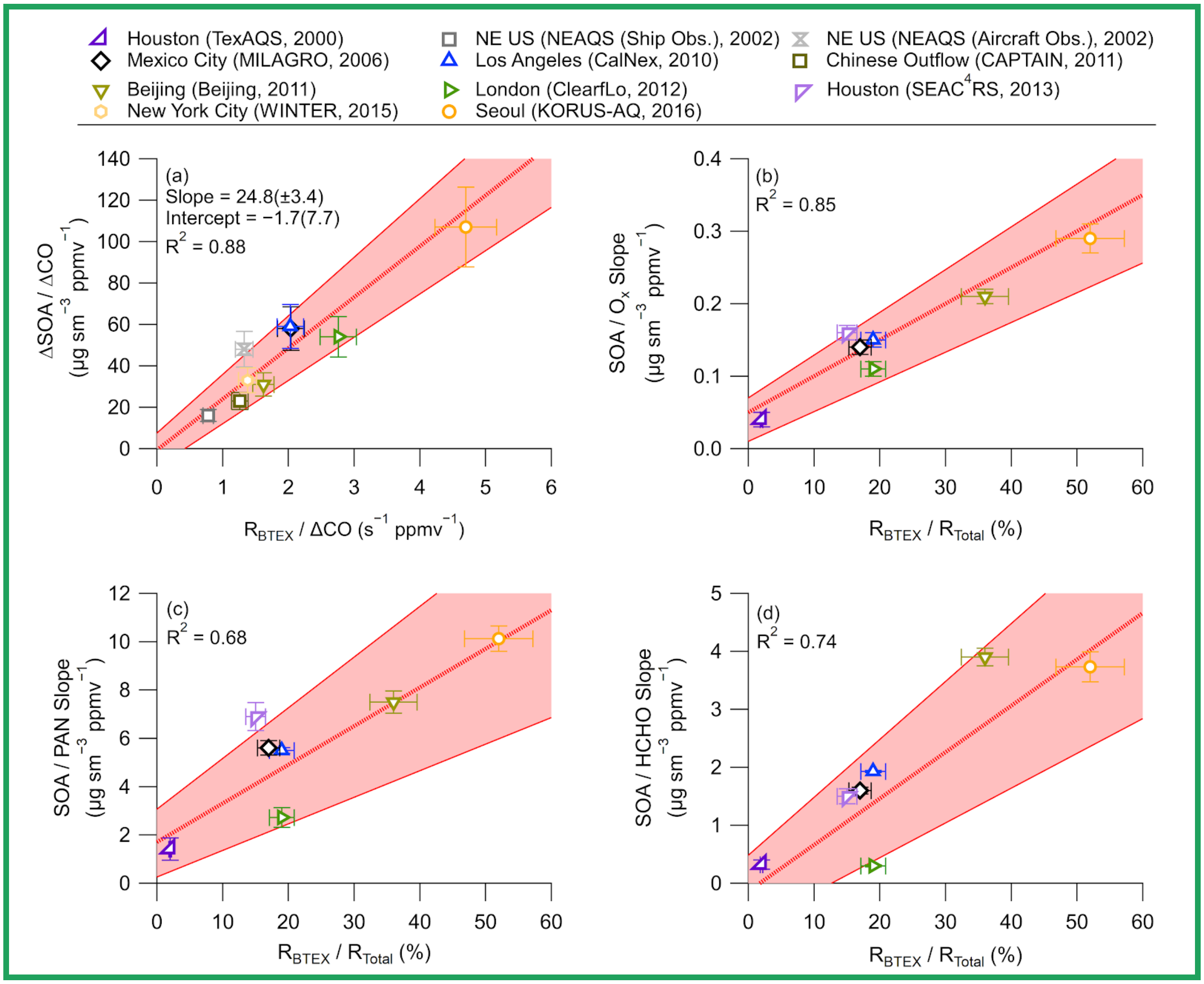

Figure 2. (a) Scatter plot of background and dilution corrected ASOA concentrations (ΔASOA/ΔCO at PA = 0.5 equivalent days) versus BTEX emission reactivity ratio (R_{BTEX}= $\boxed{\Sigma_i[\mathrm{VOC}/\mathrm{CO}]_i}$) for multiple major field campaigns on three continents. Comparison of ASOA versus (b) Ox, (c) PAN, and (d) HCHO slopes versus the ratio of the BTEX/Total emission reactivity, where total is the OH reactivity for the emissions of BTEX + C¬2-3 alkenes + C2-6 alkanes (Table S5 through Table S7), for the campaigns studied here. For all figures, red shading is the ±1σ uncertainty of the slope, and the bars are ±1σ uncertainty of the data (see Sect. S5).

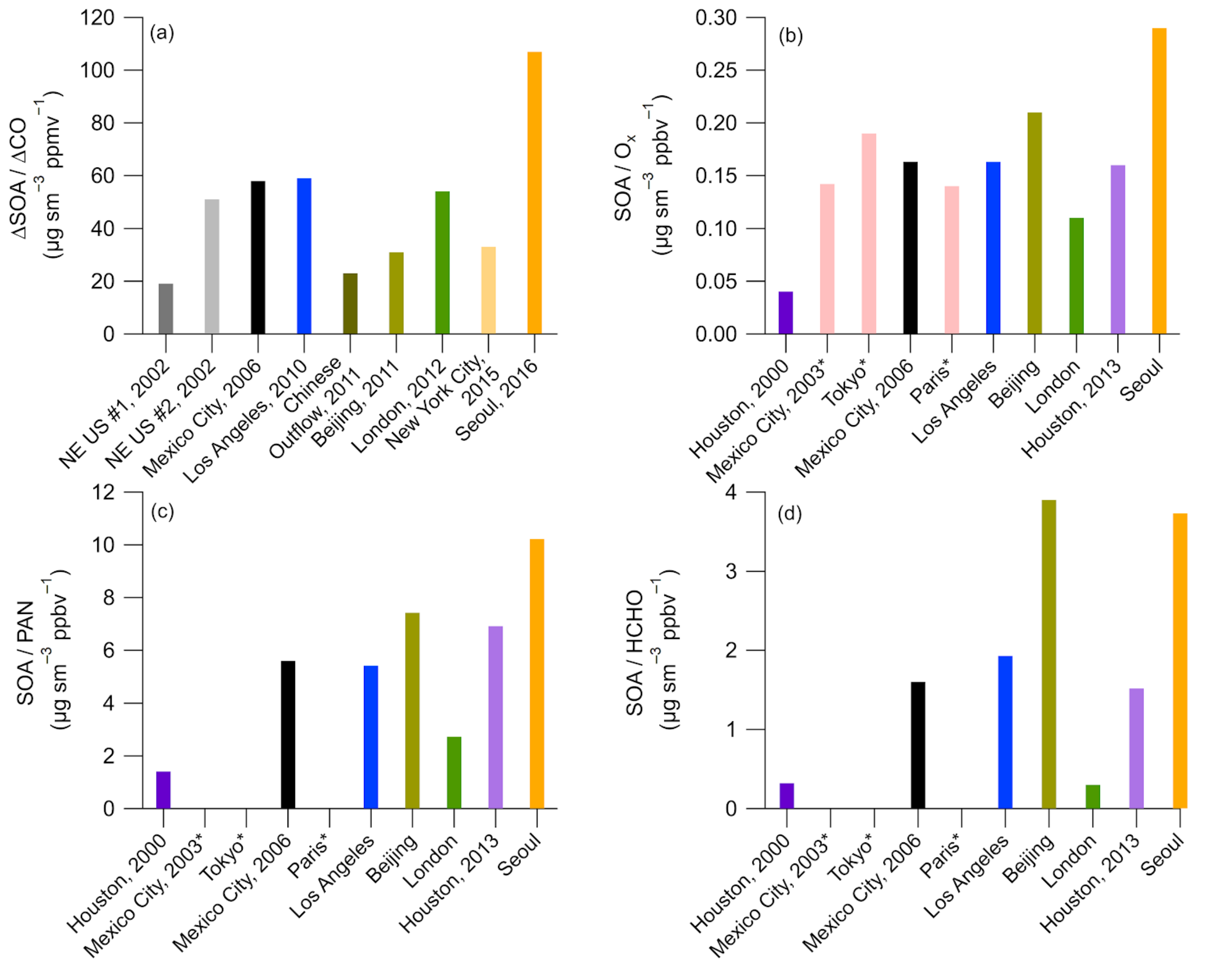

Figure 3~~24~~. (a) A comparison of the ΔSOA/ΔCO for the urban campaigns on three continents. Comparison of (b) SOA/Ox, (c) SOA/HCHO, and (d) SOA/PAN slopes for the urban areas (Table S4). For (b) through (d), cities marked with * have no HCHO, PAN, or hydrocarbon data.

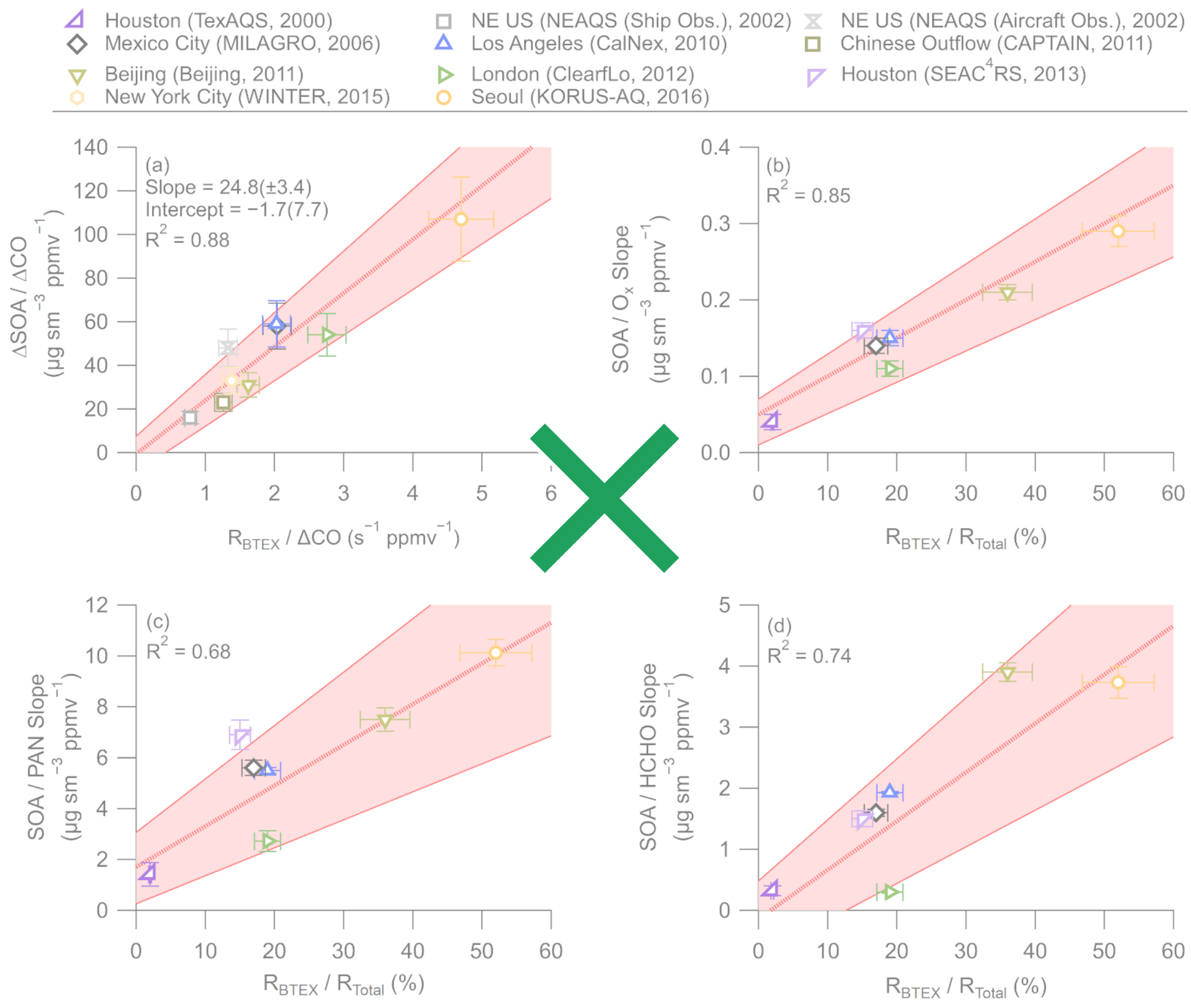

~~**Figure 35**. (a) Scatter plot of background and dilution corrected ASOA concentrations (ΔASOA/ΔCO at PA = 0.5 equivalent days) versus BTEX emission reactivity ratio ($R_{BTEX} = \sum_i [VOC/CO]_i$) for multiple major field campaigns on three continents. Comparison of ASOA versus (b) Ox, (c) PAN, and (d) HCHO slopes versus the ratio of the BTEX/Total emission reactivity, where total is the OH reactivity for the emissions of BTEX + C2-3 alkenes + C2-6 alkanes (Table S5 through Table S7), for the campaigns studied here. For all figures, red shading is the ±1σ uncertainty of the slope, and the bars are ±1σ uncertainty of the data (see Sect. 2.2S5).~~

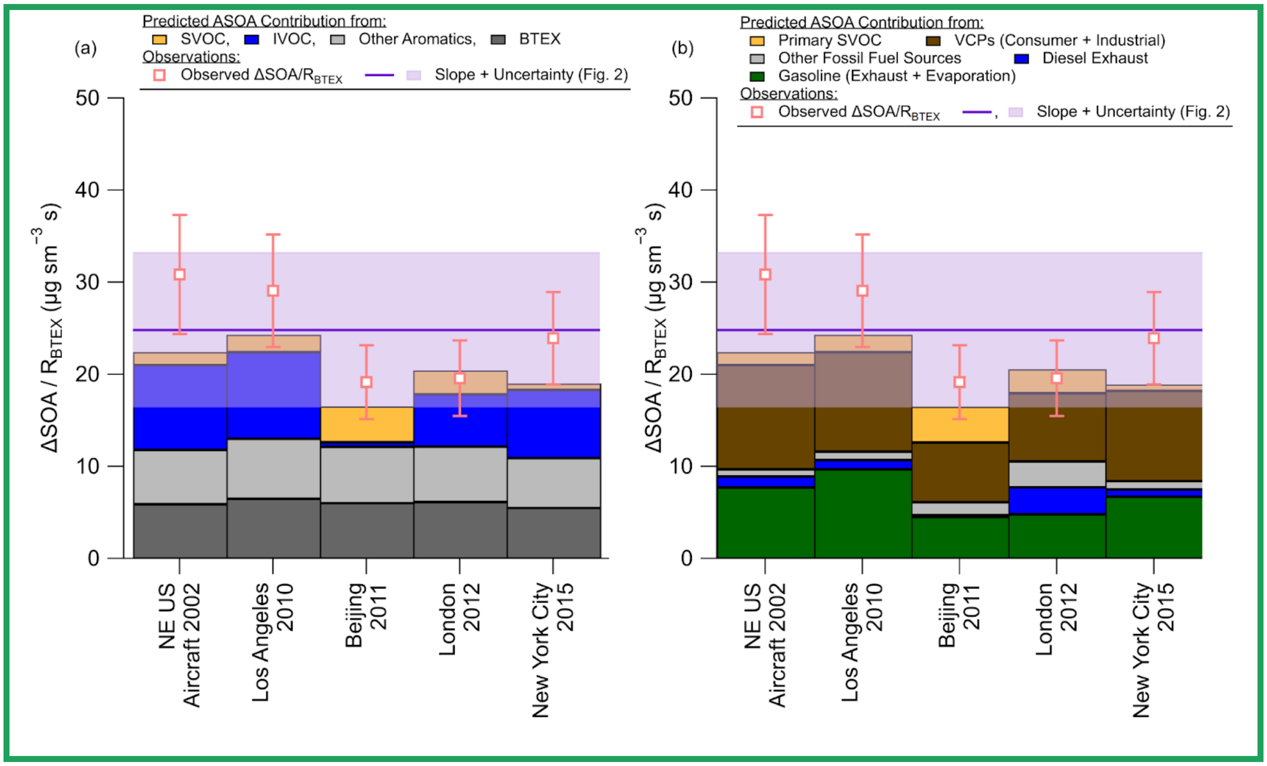

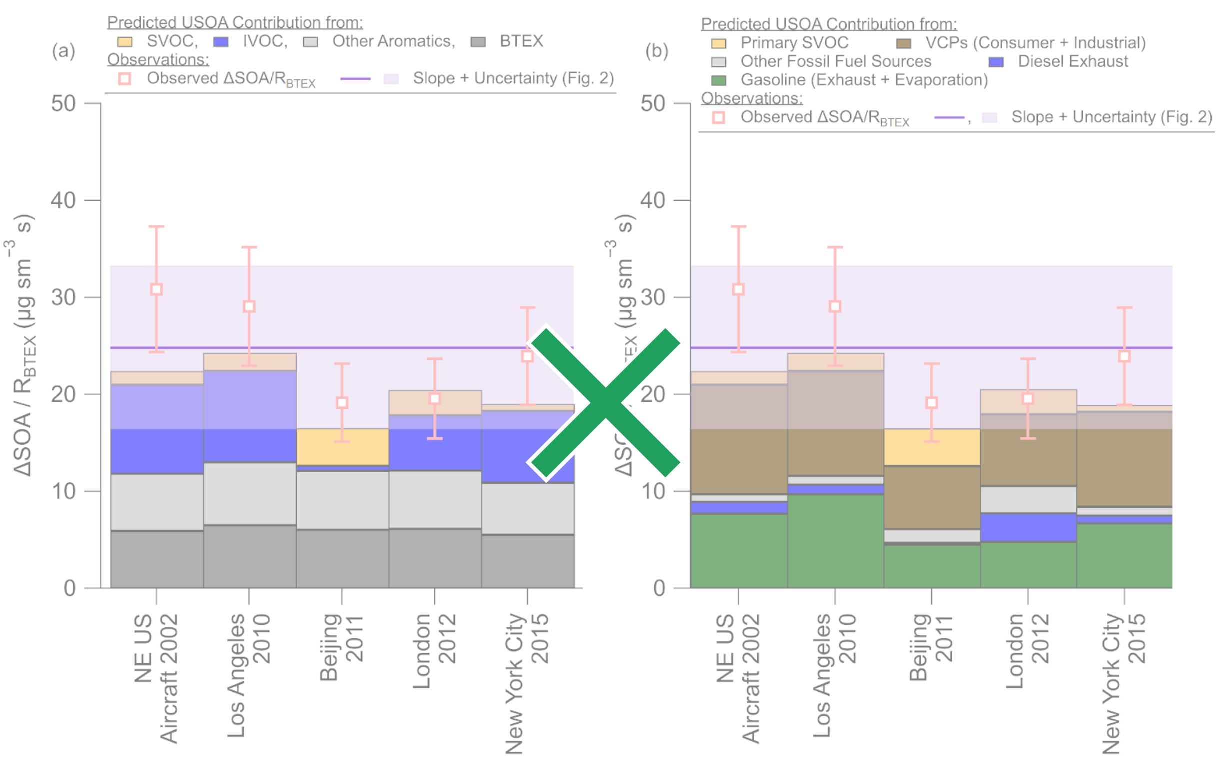

Figure 4~~6~~. (a) Budget analysis for the contribution of the observed $\Delta SOA/R_{BTEX}$ (Fig. 2~~5~~) for cities with known emissions inventories for different volatility classes (see SI and Fig. 5~~2~~ and Fig. S6~~3~~). (b) Same as (a), but for sources of emissions. For (a) and (b), SVOC is the contribution from both vehicle and other (cooking, etc.) sources. See ~~Sect. 2 and~~ SI for information about the emissions, ASOA precursor contribution, error analysis, and discussion about sensitivity of emission inventory IVOC/BTEX ratios for different cities and years in the US.

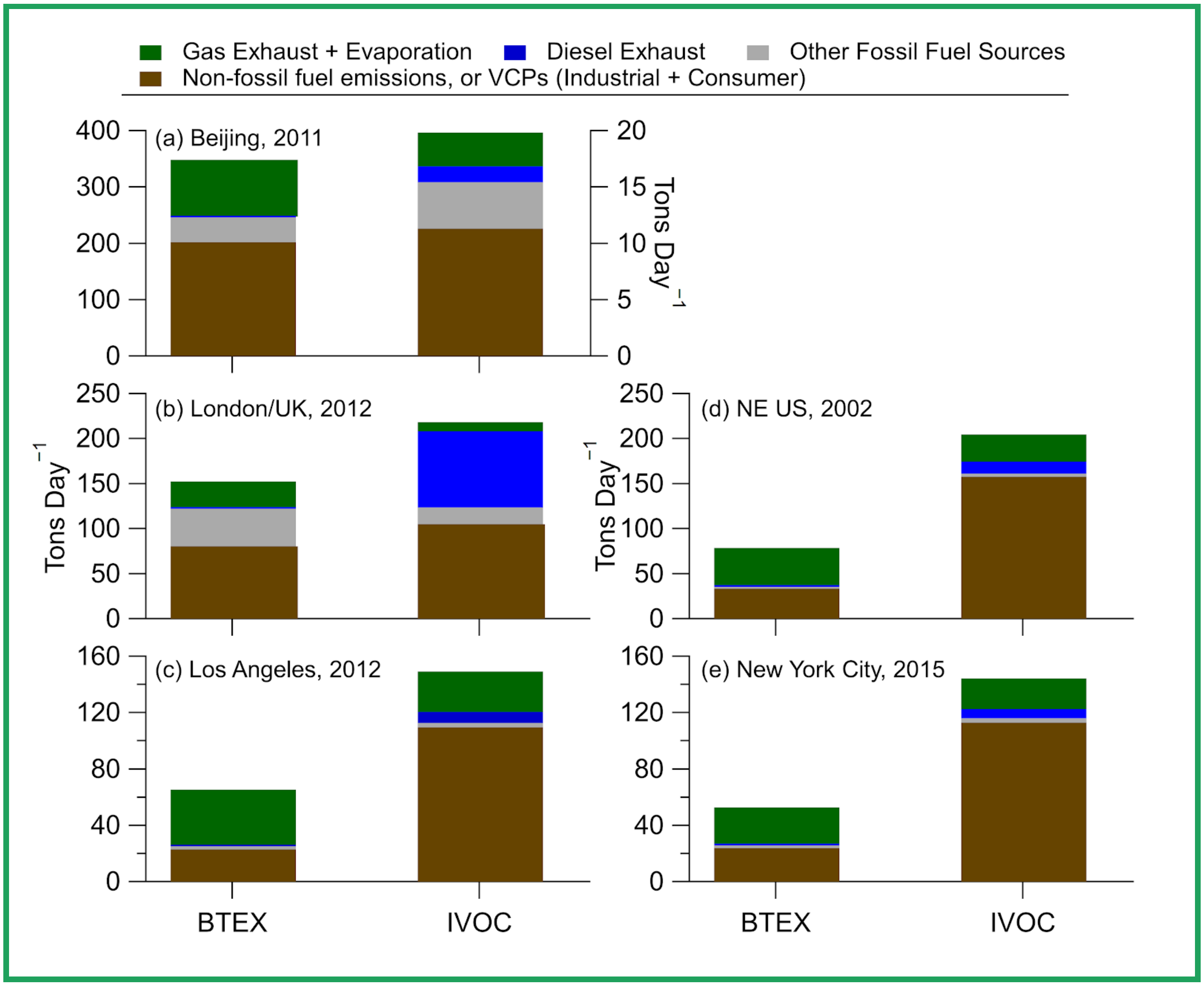

Figure 5. Comparison of BTEX and IVOC sources for (a) Beijing (see SI section about Beijing emission inventory), (b) London (see SI section about London/UK emission inventory), and (c) Los Angeles, (d) Northeast United States, and (e) New York City (see SI section about United States for (c) – (e)). For (a), BTEX is on the left axis and IVOC is on the right axis, due to the small emissions per day for IVOC.

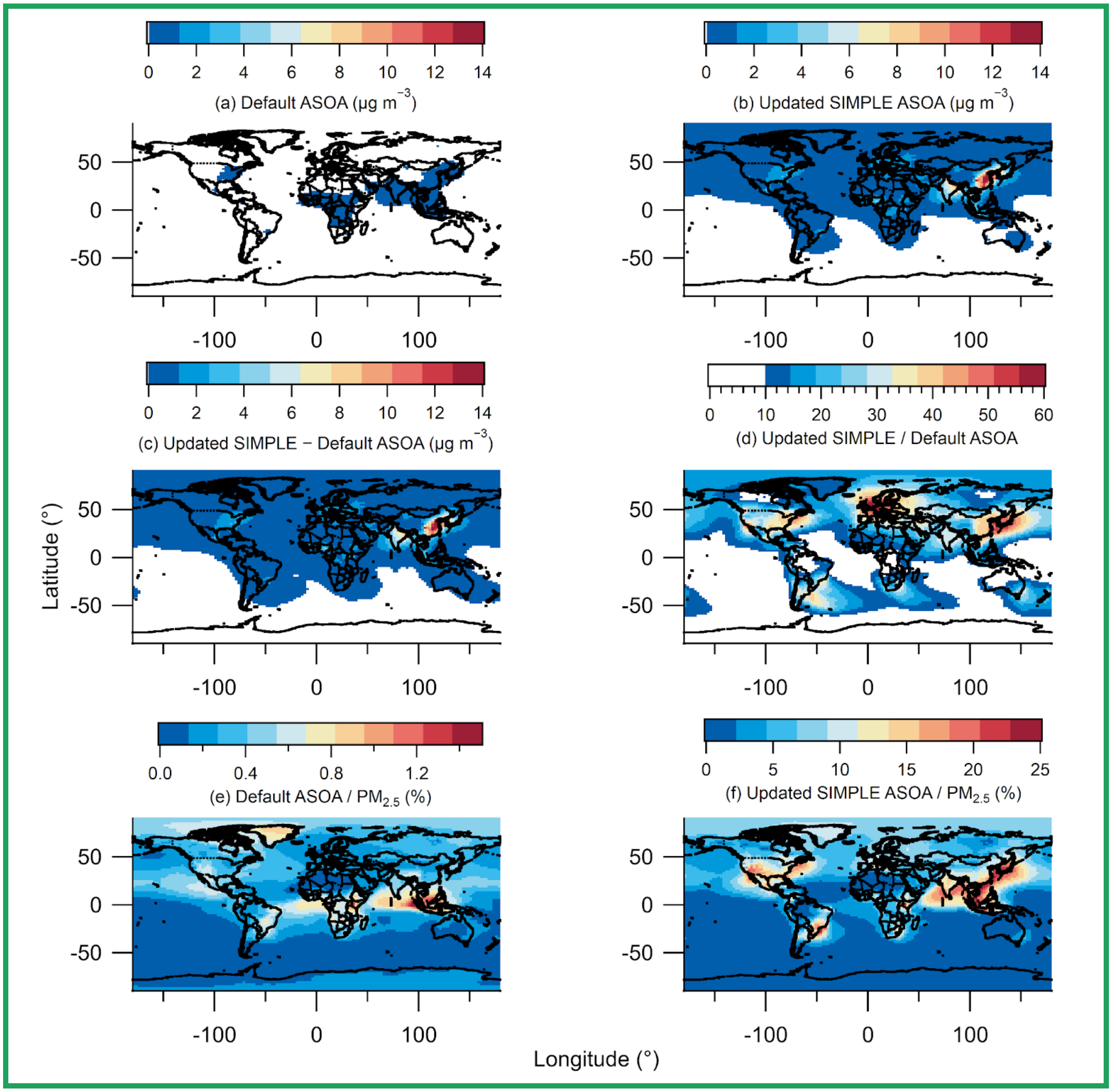

Figure 6. (a) Annual average modeled ASOA using the default VBS. (b) Annual average modeled ASOA using the updated SIMPLE model. (c) Difference between annual average modeled updated SIMPLE and default VBS. (d) Ratio between annual average modeled updated SIMPLE and default VBS. (e) Percent contribution of annual average modeled ASOA using default VBS to total modelled $PM_{2.5}$. (f) Percent contribution of annual average modeled ASOA using updated SIMPLE to total modelled $PM_{2.5}$.

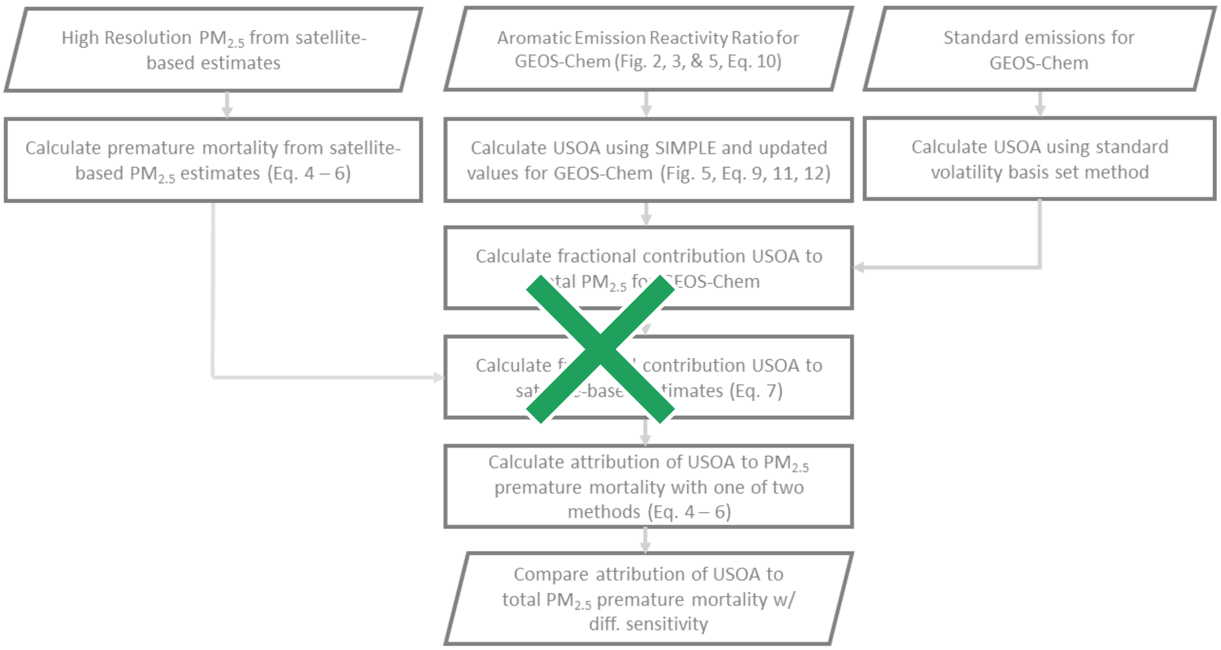

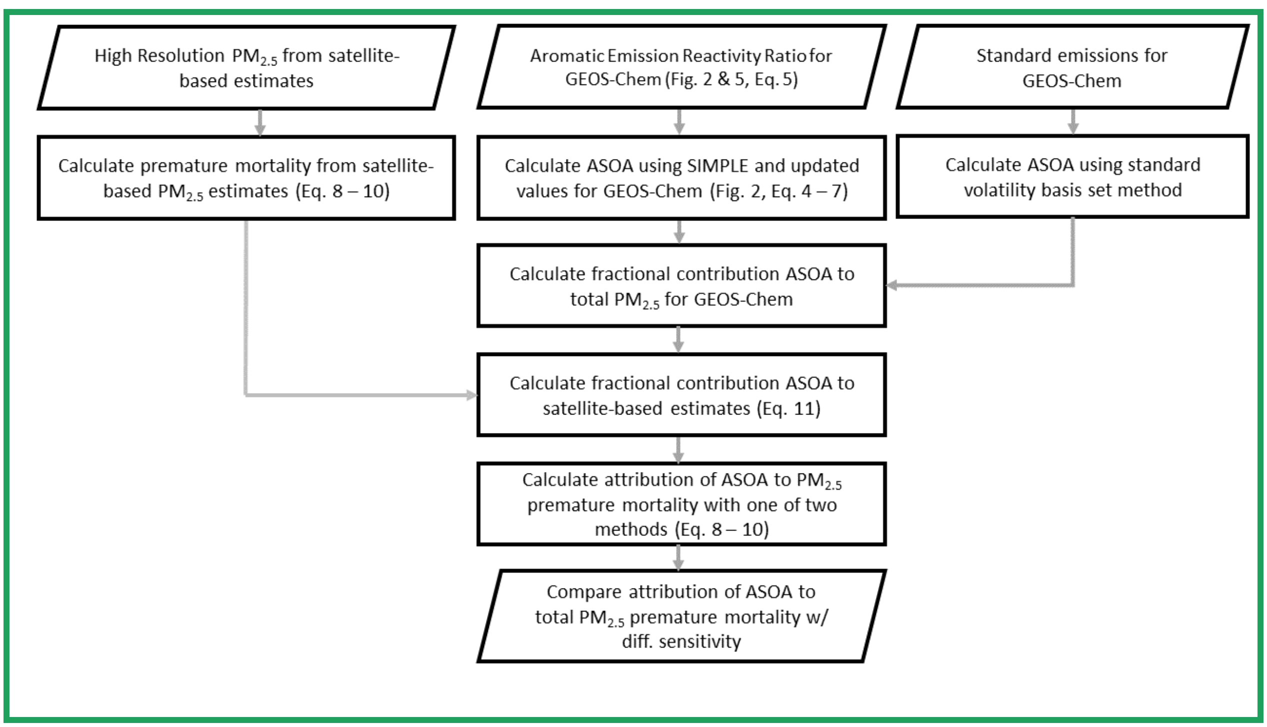

Figure 7. Flowchart describing how observed ASOA production was used to calculate ASOA in GEOS-Chem, and how the satellite-based $PM_{2.5}$ estimates and GEOS-Chem $PM_{2.5}$ speciation was used to estimate the premature mortality and attribution of premature mortality by ASOA. See Sect. 2 and SI for further information about the details in the figure. SIMPLE is described in Eq. 4~~9~~ and by Hodzic and Jimenez (2011) and Hayes et al. (2015). The one of two methods mentioned include either the Integrated Exposure-Response (IER) (Burnett et al., 2014) with

Global Burden of Disease (GBD) dataset (IHME, 2016) or the new Global Exposure Mortality Model (GEMM) (Burnett et al., 2018) methods. For both IER and GEMM, the marginal method (Silva et al., 2016) or attributable fraction method (Anenberg et al., 2019) are used.

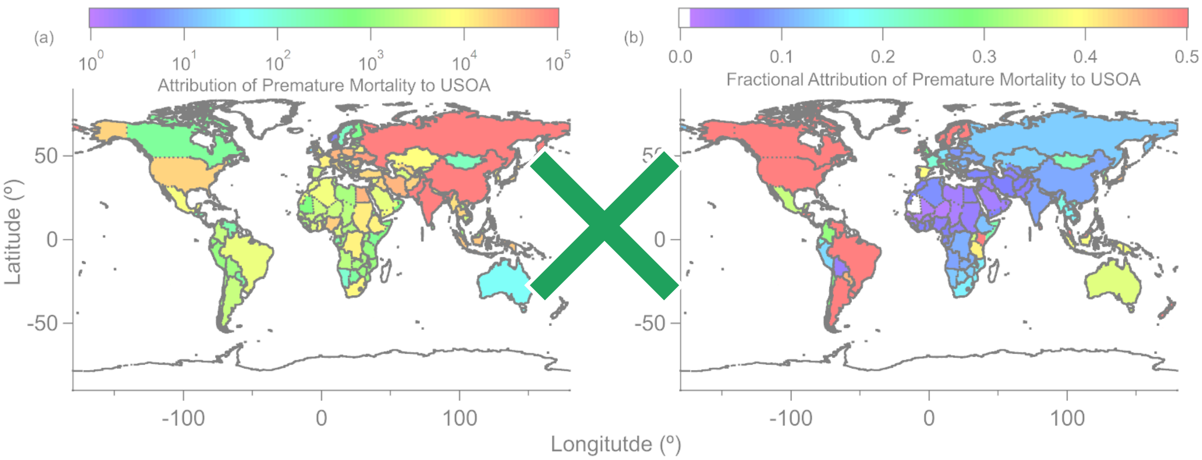

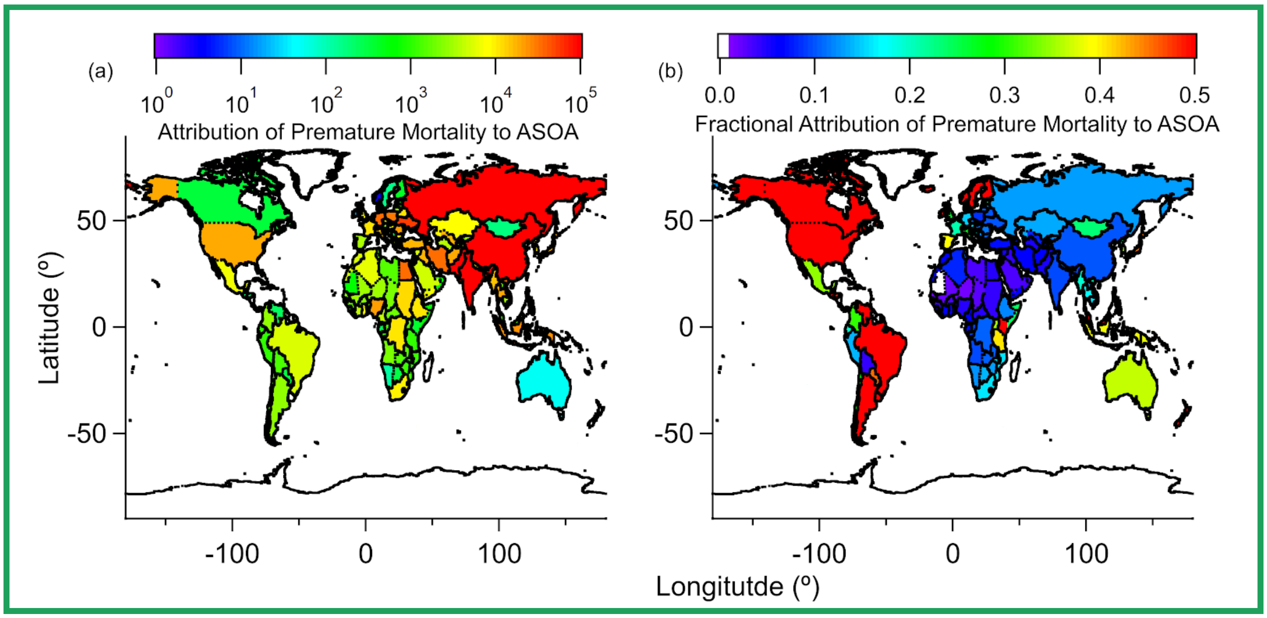

Figure 8. Five-year average (a) estimated reduction in $PM_{2.5}$-associated premature deaths, by country, upon removing ASOA from total $PM_{2.5}$, and (b) fractional reduction (reduction $PM_{2.5}$ premature deaths / total $PM_{2.5}$ premature deaths) in $PM_{2.5}$-associated premature deaths, by country, upon removing ASOA from GEOS-Chem. The IER methods are used here. See Fig. S9~~7~~ and Fig. S12~~0~~ for results using GEMM. See Fig. S10~~8~~ for 10×10 km^2 area results in comparison with country-level results.

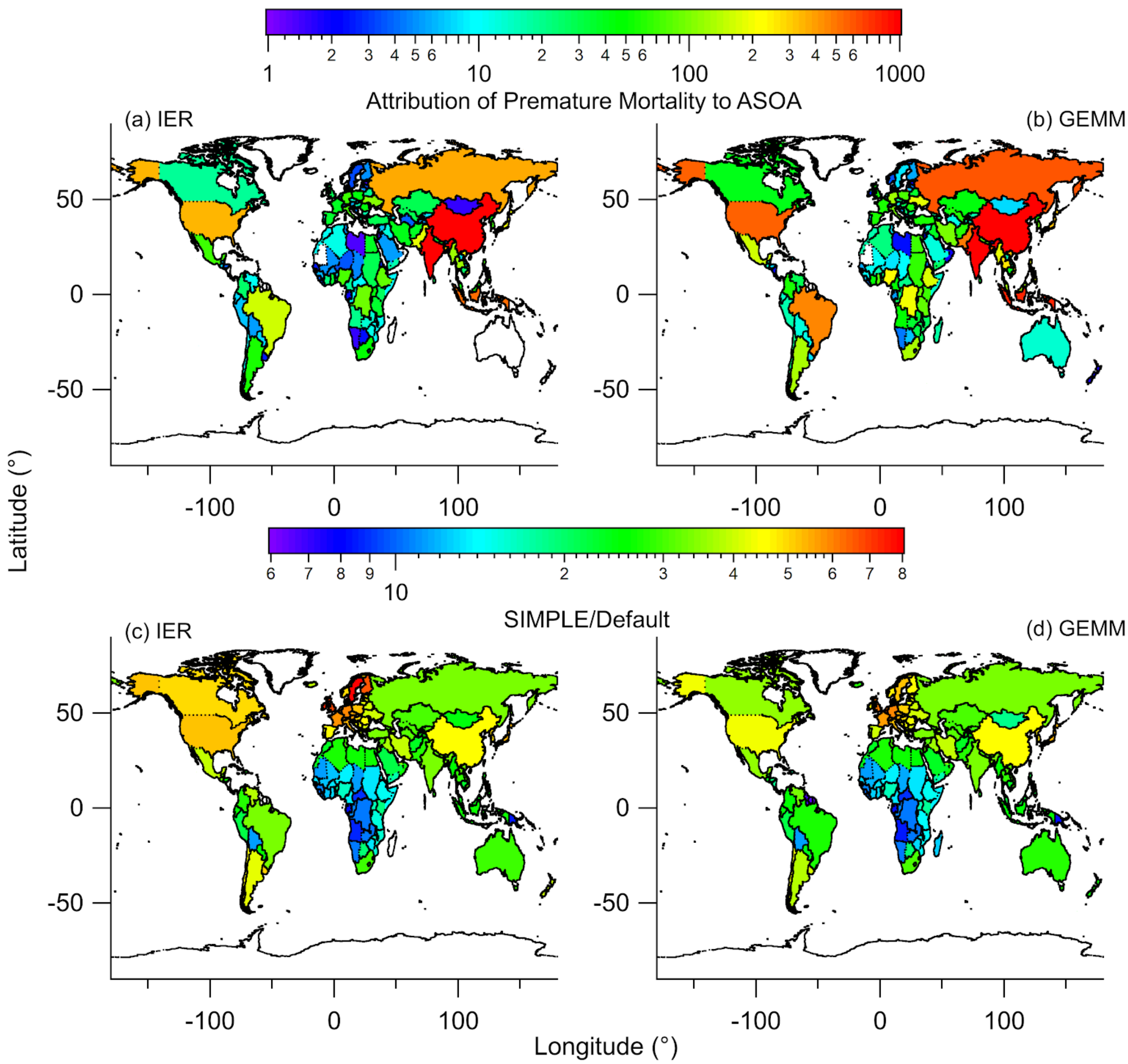

Figure 9. Attribution of premature mortality to ASOA using (a) IER or (b) GEMM, using the non-volatile primary OA and traditional SOA precursors method in prior studies (e.g., Ridley et al., 2018). The increase in attribution of premature mortality to ASOA for the "SIMPLE" model (Fig. 8) versus the non-volatile primary OA and traditional SOA precursor method ("Default"), for (c) IER and (d) GEMM.

Table 1. List of campaigns used here. For values previously reported for those campaigns, they are noted. For Seasons, W = Winter, Sp = Spring, and Su = Summer.

Location	Field Campaign	Coordinates		Time Period	Season	Previous Publication/Campaign Overview
		Long. (°)	Lat. (°)			
Houston, TX, USA (2000)	TexAQS 2000	−95.4	29.8	15/Aug/2000 - 15/Sept/2000	Su	Jimenez et al. (2009)[a], Wood et al. (2010)[b]
Northeast USA (2002)	NEAQS 2002	−78.1 - −70.5	32.8 - 43.1	26/July/2002; 29/July/2002 - 10/Aug/2002	Su	Jimenez et al. (2009)[a], de Gouw and Jimenez (2009)[c], Kleinman et al. (2007)[c]
Mexico City, Mexico (2003)	MCMA-2003	−99.2	19.5	31/Mar/2003 - 04/May/2003	Sp	Molina et al. (2007), Herndon et al. (2008)[b]
Tokyo, Japan (2004)		139.7	35.7	24/July/2004 - 14/Aug/2004	Su	Kondo et al. (2008)[a], Miyakawa et al. (2008)[a], Morino et al. (2014)[b]
Mexico City, Mexico (2006)	MILAGRO	−99.4 - −98.6	19.0 − 19.8	04/Mar/2006 - 29/Mar/2006	Sp	Molina et al. (2010), DeCarlo et al. (2008)[a], Wood et al. (2010)[b], DeCarlo et al. (2010)[c]
Paris, France (2009)	MEGAPOLI	48.9	2.4	13/July/2009 - 29/July/2009	Su	Freney et al. (2014)[a], Zhang et al. (2015)[b]
Pasadena, CA, USA (2010)	CalNex	−118.1	34.1	15/May/2010 - 16/June/2010	Sp	Ryerson et al. (2013), Hayes et al. (2013)[a,b,c]
Changdao Island, China (2011)	CAPTAIN	120.7	38.0	21/Mar/2011 - 24/Apr/2011	Sp	Hu et al. (2013)[a,c]
Beijing, China (2011)	CareBeijing 2011	116.4	39.9	03/Aug/2011 - 15/Sept/2011	Su	Hu et al. (2016)[a,b,c]
London, UK (2012)	ClearfLo	0.1	51.5	22/July/2012 - 18/Aug/2012	Su	Bohnenstengel et al. (2015)
Houston, TX, USA (2013)	SEAC^{4}RS	−96.0 - −94.0	29.2 - 30.3	01/Aug/2013 - 23/Sept/2013	Su	Toon et al. (2016)
New York City, NY, USA (2015)	WINTER	−74.0 - −69.0	39.5 - 42.5	07/Feb/2015	W	Schroder et al. (2018)[a,c]
Seoul, South Korea (2016)	KORUS-AQ	124.6 - 128.0	36.8 - 37.6	01/May/2016 - 10/June/2016	Sp	Nault et al. (2018)[a,b,c,d]

[a]Reference used for PM_1 composition. [b]Reference used for SOA/O_x slope. [c]Reference used for ΔOA/ΔCO value. [d]Reference used for SOA/HCHO and SOA/PAN slopes

References

Anenberg, S., Miller, J., Henze, D. and Minjares, R.: A global snapshot of the air pollution-related health impacts of transportation sector emissions in 2010 and 2015, ICCT, Climate & Clean Air Coalition., 2019.

Atkinson, R. and Arey, J.: Atmospheric Degradation of Volatile Organic Compounds, Chem. Rev., 103, 4605–4638, 2003.

Atkinson, R., Baulch, D. L., Cox, R. A., Crowley, J. N., Hampson, R. F., Hynes, R. G., Jenkin, M. E., Rossi, M. J., Troe, J. and IUPAC Subcommittee: Evaluated kinetic and photochemical data for atmospheric chemistry: Volume II - gas phase reactions of organic species, Atmos. Chem. Phys., 6(11), 3625–4055, 2006.

Bae, M.-S., Demerjian, K. L. and Schwab, J. J.: Seasonal estimation of organic mass to organic carbon in PM2.5 at rural and urban locations in New York state, Atmos. Environ., 40(39), 7467–7479, 2006.

Bahreini, R., Ervens, B., Middlebrook, A. M., Warneke, C., de Gouw, J. A., DeCarlo, P. F., Jimenez, J. L., Brock, C. A., Neuman, J. A., Ryerson, T. B., Stark, H., Atlas, E., Brioude, J., Fried, A., Holloway, J. S., Peischl, J., Richter, D., Walega, J., Weibring, P., Wollny, A. G. and Fehsenfeld, F. C.: Organic aerosol formation in urban and industrial plumes near Houston and Dallas, Texas, J. Geophys. Res., 114, 1185, 2009.

Bertram, T. H., Perring, A. E., Wooldridge, P. J., Crounse, J. D., Kwan, A. J., Wennberg, P. O., Scheuer, E., Dibb, J., Avery, M., Sachse, G., Vay, S. A., Crawford, J. H., McNaughton, C. S., Clarke, A., Pickering, K. E., Fuelberg, H., Huey, G., Blake, D. R., Singh, H. B., Hall, S. R., Shetter, R. E., Fried, A., Heikes, B. G. and Cohen, R. C.: Direct Measurements of the Convective Recycling of the Upper Troposphere, Science, 315(5813), 816–820, 2007.

Bey, I., Jacob, D. J., Yantosca, R. M., Logan, J. A., Field, B. D., Fiore, A. M., Li, Q., Liu, H. Y., Mickley, L. J. and Schultz, M. G.: Global modeling of tropospheric chemistry with assimilated meteorology: Model description and evaluation, J. Geophys. Res. D: Atmos., 106(D19), 23073–23095, 2001.

Bohnenstengel, S. I., Belcher, S. E., Aiken, A., Allan, J. D., Allen, G., Bacak, A., Bannan, T. J., Barlow, J. F., Beddows, D. C. S., Bloss, W. J., Booth, A. M., Chemel, C., Coceal, O., Di Marco, C. F., Dubey, M. K., Faloon, K. H., Fleming, Z. L., Furger, M., Gietl, J. K., Graves, R. R., Green, D. C., Grimmond, C. S. B., Halios, C. H., Hamilton, J. F., Harrison, R. M., Heal, M. R., Heard, D. E., Helfter, C., Herndon, S. C., Holmes, R. E., Hopkins, J. R., Jones, A. M., Kelly, F. J., Kotthaus, S., Langford, B., Lee, J. D., Leigh, R. J., Lewis, A. C., Lidster, R. T., Lopez-Hilfiker, F. D., McQuaid, J. B., Mohr, C., Monks, P. S., Nemitz, E., Ng, N. L., Percival, C. J., Prévôt, A. S. H., Ricketts, H. M. A., Sokhi, R., Stone, D., Thornton, J. A., Tremper, A. H., Valach, A. C., Visser, S., Whalley, L. K., Williams, L. R., Xu, L., Young, D. E., Zotter, P., Bohnenstengel, S. I., Belcher, S. E., Aiken, A., Allan, J. D., Allen, G., Bacak, A., Bannan, T. J., Barlow, J. F., Beddows, D. C. S., Bloss, W. J., Booth, A. M., Chemel, C., Coceal, O., Marco, C. F. D., Dubey,

M. K., Faloon, K. H., Fleming, Z. L., Furger, M., Gietl, J. K., Graves, R. R., Green, D. C., Grimmond, C. S. B., Halios, C. H., Hamilton, J. F., Harrison, R. M., Heal, M. R., Heard, D. E., Helfter, C., Herndon, S. C., Holmes, R. E., Hopkins, J. R., Jones, A. M., Kelly, F. J., Kotthaus, S., Langford, B., Lee, J. D., Leigh, R. J., Lewis, A. C., Lidster, R. T., Lopez-Hilfiker, F. D., et al.: Meteorology, Air Quality, and Health in London: The ClearfLo Project, Bull. Am. Meteorol. Soc., 96(5), 779–804, 2015.

Burnett, R., Chen, H., Szyszkowicz, M., Fann, N., Hubbell, B., Pope, C. A., Apte, J. S., Brauer, M., Cohen, A., Weichenthal, S., Coggins, J., Di, Q., Brunekreef, B., Frostad, J., Lim, S. S., Kan, H., Walker, K. D., Thurston, G. D., Hayes, R. B., Lim, C. C., Turner, M. C., Jerrett, M., Krewski, D., Gapstur, S. M., Diver, W. R., Ostro, B., Goldberg, D., Crouse, D. L., Martin, R. V., Peters, P., Pinault, L., Tjepkema, M., van Donkelaar, A., Villeneuve, P. J., Miller, A. B., Yin, P., Zhou, M., Wang, L., Janssen, N. A. H., Marra, M., Atkinson, R. W., Tsang, H., Quoc Thach, T., Cannon, J. B., Allen, R. T., Hart, J. E., Laden, F., Cesaroni, G., Forastiere, F., Weinmayr, G., Jaensch, A., Nagel, G., Concin, H. and Spadaro, J. V.: Global estimates of mortality associated with long-term exposure to outdoor fine particulate matter, Proc. Natl. Acad. Sci. U. S. A., 115(38), 9592–9597, 2018.

Burnett, R. T., Pope, C. A., Ezzati, M., Olives, C., Lim, S. S., Mehta, S., Shin, H. H., Singh, G., Hubbell, B., Brauer, M., Anderson, H. R., Smith, K. R., Balmes, J. R., Bruce, N. G., Kan, H., Laden, F., Prüss-Ustün, A., Turner, M. C., Gapstur, S. M., Diver, W. R. and Cohen, A.: An integrated risk function for estimating the global burden of disease attributable to ambient fine particulate matter exposure, Environ. Health Perspect., 122(4), 397–403, 2014.

CIESIN: Gridded Population of the World (GPW), v4, SEDAC [online] Available from: https://sedac.ciesin.columbia.edu/data/collection/gpw-v4 (Accessed 12 May 2020), 2017.

Coggon, M. M., McDonald, B. C., Vlasenko, A., Veres, P. R., Bernard, F., Koss, A. R., Yuan, B., Gilman, J. B., Peischl, J., Aikin, K. C., DuRant, J., Warneke, C., Li, S.-M. and de Gouw, J. A.: Diurnal Variability and Emission Pattern of Decamethylcyclopentasiloxane (D_5) from the Application of Personal Care Products in Two North American Cities, Environ. Sci. Technol., 52(10), 5610–5618, 2018.

Cohen, A. J., Brauer, M., Burnett, R., Anderson, H. R., Frostad, J., Estep, K., Balakrishnan, K., Brunekreef, B., Dandona, L., Dandona, R., Feigin, V., Freedman, G., Hubbell, B., Jobling, A., Kan, H., Knibbs, L., Liu, Y., Martin, R., Morawska, L., Pope, C. A., Shin, H., Straif, K., Shaddick, G., Thomas, M., van Dingenen, R., van Donkelaar, A., Vos, T., Murray, C. J. L. and Forouzanfar, M. H.: Estimates and 25-year trends of the global burden of disease attributable to ambient air pollution: an analysis of data from the Global Burden of Diseases Study 2015, Lancet, 389(10082), 1907–1918, 2017.

DeCarlo, P. F., Dunlea, E. J., Kimmel, J. R., Aiken, A. C., Sueper, D., Crounse, J., Wennberg, P. O., Emmons, L., Shinozuka, Y., Clarke, A., Zhou, J., Tomlinson, J., Collins, D. R., Knapp, D., Weinheimer, A. J., Montzka, D. D., Campos, T. and Jimenez, J. L.: Fast airborne aerosol size and chemistry measurements above Mexico City and Central Mexico during the MILAGRO campaign, Atmos. Chem. Phys., 8(14), 4027–4048, 2008.

DeCarlo, P. F., Ulbrich, I. M., Crounse, J., de Foy, B., Dunlea, E. J., Aiken, A. C., Knapp, D., Weinheimer, A. J., Campos, T., Wennberg, P. O. and Jimenez, J. L.: Investigation of the sources and processing of organic aerosol over the Central Mexican Plateau from aircraft measurements during MILAGRO, Atmos. Chem. Phys., 10(12), 5257–5280, 2010.

Dominutti, P., Keita, S., Bahino, J., Colomb, A., Liousse, C., Yoboué, V., Galy-Lacaux, C., Morris, E., Bouvier, L., Sauvage, S. and Borbon, A.: Anthropogenic VOCs in Abidjan, southern West Africa: from source quantification to atmospheric impacts, Atmos. Chem. Phys., 19(18), 11721–11741, 2019.

van Donkelaar, A., Martin, R. V., Brauer, M. and Boys, B. L.: Use of Satellite Observations for Long-Term Exposure Assessment of Global Concentrations of Fine Particulate Matter, Environ. Health Perspect., 123(2), 135–143, 2015.

van Donkelaar, A., Martin, R. V., Brauer, M., Hsu, N. C., Kahn, R. A., Levy, R. C., Lyapustin, A., Sayer, A. M. and Winker, D. M.: Global Estimates of Fine Particulate Matter using a Combined Geophysical-Statistical Method with Information from Satellites, Models, and Monitors, Environ. Sci. Technol., 50(7), 3762–3772, 2016.

Duncan Fairlie, T., Jacob, D. J. and Park, R. J.: The impact of transpacific transport of mineral dust in the United States, Atmos. Environ., 41(6), 1251–1266, 2007.

Dzepina, K., Volkamer, R. M., Madronich, S., Tulet, P., Ulbrich, I. M., Zhang, Q., Cappa, C. D., Ziemann, P. J. and Jimenez, J. L.: Evaluation of recently-proposed secondary organic aerosol models for a case study in Mexico City, Atmos. Chem. Phys., 9(15), 5681–5709, 2009.

EMEP/EEA: EMEP/EEA Air Pollutant Emission Inventory Guidebook 2016, EEA, Luxembourg., 2016.

Ensberg, J. J., Hayes, P. L., Jimenez, J. L., Gilman, J. B., Kuster, W. C., de Gouw, J. A., Holloway, J. S., Gordon, T. D., Jathar, S., Robinson, A. L. and Seinfeld, J. H.: Emission factor ratios, SOA mass yields, and the impact of vehicular emissions on SOA formation, Atmos. Chem. Phys., 14(5), 2383–2397, 2014.

Freney, E. J., Sellegri, K., Canonaco, F., Colomb, A., Borbon, A., Michoud, V., Crumeyrolle, S., Amarouche, N., Bourianne, T., Gomes, L., Prevot, A. S. H., Beekmann, M. and Schwarzenböeck, A.: Characterizing the impact of urban emissions on regional aerosol particles: Airborne measurements during the MEGAPOLI experiment, Atmos. Chem. Phys., 14(3), 1397–1412, 2014.

Gentner, D. R., Isaacman, G., Worton, D. R., Chan, A. W. H., Dallmann, T. R., Davis, L., Liu, S., Day, D. A., Russell, L. M., Wilson, K. R., Weber, R., Guha, A., Harley, R. A. and Goldstein, A. H.: Elucidating secondary organic aerosol from diesel and gasoline vehicles through detailed characterization of organic carbon emissions, Proc. Natl. Acad. Sci. U. S. A., 109(45),

18318–18323, 2012.

Goel, R. and Guttikunda, S. K.: Evolution of on-road vehicle exhaust emissions in Delhi, Atmos. Environ., 105, 78–90, 2015.

de Gouw, J. A. and Jimenez, J. L.: Organic Aerosols in the Earth's Atmosphere, Environ. Sci. Technol., 43(20), 7614–7618, 2009.

de Gouw, J. A., Middlebrook, A. M., Warneke, C., Goldan, P. D., Kuster, W. C., Roberts, J. M., Fehsenfeld, F. C., Worsnop, D. R., Canagaratna, M. R., Pszenny, A. A. P., Keene, W. C., Marchewka, M., Bertman, S. B. and Bates, T. S.: Budget of organic carbon in a polluted atmosphere: Results from the New England Air Quality Study in 2002, J. Geophys. Res. D: Atmos., 110(16), 1–22, 2005.

de Gouw, J. A., Gilman, J. B., Kim, S.-W., Lerner, B. M., Isaacman-VanWertz, G., McDonald, B. C., Warneke, C., Kuster, W. C., Lefer, B. L., Griffith, S. M., Dusanter, S., Stevens, P. S. and Stutz, J.: Chemistry of Volatile Organic Compounds in the Los Angeles basin: Nighttime Removal of Alkenes and Determination of Emission Ratios, J. Geophys. Res.: Atmos., 122(21), 11,843–11,861, 2017.

Grieshop, A. P., Logue, J. M., Donahue, N. M. and Robinson, A. L.: Laboratory investigation of photochemical oxidation of organic aerosol from wood fires 1: measurement and simulation of organic aerosol evolution, Atmos. Chem. Phys., 9(4), 1263–1277, 2009.

Hallquist, M., Wenger, J. C., Baltensperger, U., Rudich, Y., Simpson, D., Claeys, M., Dommen, J., Donahue, N. M., George, C., Goldstein, A. H., Hamilton, J. F., Herrmann, H., Hoffmann, T., Iinuma, Y., Jang, M., Jenkin, M. E., Jimenez, J. L., Kiendler-Scharr, A., Maenhaut, W., McFiggans, G., Mentel, T. F., Monod, A., Prévôt, A. S. H., Seinfeld, J. H., Surratt, J. D., Szmigielski, R. and Wildt, J.: The formation, properties and impact of secondary organic aerosol: current and emerging issues, Atmos. Chem. Phys., 9(14), 5155–5236, 2009.

Hayes, P. L., Ortega, A. M., Cubison, M. J., Froyd, K. D., Zhao, Y., Cliff, S. S., Hu, W. W., Toohey, D. W., Flynn, J. H., Lefer, B. L., Grossberg, N., Alvarez, S., Rappenglück, B., Taylor, J. W., Allan, J. D., Holloway, J. S., Gilman, J. B., Kuster, W. C., de Gouw, J. A., Massoli, P., Zhang, X., Liu, J., Weber, R. J., Corrigan, A. L., Russell, L. M., Isaacman, G., Worton, D. R., Kreisberg, N. M., Goldstein, A. H., Thalman, R., Waxman, E. M., Volkamer, R., Lin, Y. H., Surratt, J. D., Kleindienst, T. E., Offenberg, J. H., Dusanter, S., Griffith, S., Stevens, P. S., Brioude, J., Angevine, W. M. and Jimenez, J. L.: Organic aerosol composition and sources in Pasadena, California, during the 2010 CalNex campaign, J. Geophys. Res. D: Atmos., 118(16), 9233–9257, 2013.

Hayes, P. L., Carlton, A. G., Baker, K. R., Ahmadov, R., Washenfelder, R. A., Alvarez, S., Rappenglück, B., Gilman, J. B., Kuster, W. C., de Gouw, J. A., Zotter, P., Prévôt, A. S. H., Szidat, S., Kleindienst, T. E., Ma, P. K. and Jimenez, J. L.: Modeling the formation and aging of secondary organic aerosols in Los Angeles during CalNex 2010, Atmos. Chem. Phys., 15(10),

5773–5801, 2015.

Heringa, M. F., DeCarlo, P. F., Chirico, R., Tritscher, T., Dommen, J., Weingartner, E., Richter, R., Wehrle, G., Prévôt, A. S. H. and Baltensperger, U.: Investigations of primary and secondary particulate matter of different wood combustion appliances with a high-resolution time-of-flight aerosol mass spectrometer, Atmos. Chem. Phys., 11(12), 5945–5957, 2011.

Herndon, S. C., Onasch, T. B., Wood, E. C., Kroll, J. H., Canagaratna, M. R., Jayne, J. T., Zavala, M. A., Knighton, W. B., Mazzoleni, C., Dubey, M. K., Ulbrich, I. M., Jimenez, J. L., Seila, R., de Gouw, J. A., de Foy, B., Fast, J., Molina, L. T., Kolb, C. E. and Worsnop, D. R.: Correlation of secondary organic aerosol with odd oxygen in Mexico City, Geophys. Res. Lett., 35(15), L15804, 2008.

Hodzic, A. and Jimenez, J. L.: Modeling anthropogenically controlled secondary organic aerosols in a megacity: A simplified framework for global and climate models, Geosci. Model Dev., 4(4), 901–917, 2011.

Hodzic, A., Jimenez, J. L., Madronich, S., Aiken, A. C., Bessagnet, B., Curci, G., Fast, J., Lamarque, J.-F., Onasch, T. B., Roux, G., Schauer, J. J., Stone, E. A. and Ulbrich, I. M.: Modeling organic aerosols during MILAGRO: importance of biogenic secondary organic aerosols, Atmos. Chem. Phys., 9(18), 6949–6981, 2009.

Hodzic, A., Jimenez, J. L., Prévôt, A. S. H., Szidat, S., Fast, J. D. and Madronich, S.: Can 3-D models explain the observed fractions of fossil and non-fossil carbon in and near Mexico City?, Atmos. Chem. Phys., 10(22), 10997–11016, 2010a.

Hodzic, A., Jimenez, J. L., Madronich, S., Canagaratna, M. R., DeCarlo, P. F., Kleinman, L. and Fast, J.: Modeling organic aerosols in a megacity: potential contribution of semi-volatile and intermediate volatility primary organic compounds to secondary organic aerosol formation, Atmos. Chem. Phys., 10(12), 5491–5514, 2010b.

Hu, W., Hu, M., Hu, W., Jimenez, J. L., Yuan, B., Chen, W., Wang, M., Wu, Y., Chen, C., Wang, Z., Peng, J., Zeng, L. and Shao, M.: Chemical composition, sources, and aging process of submicron aerosols in Beijing: Contrast between summer and winter, J. Geophys. Res. D: Atmos., 121(4), 1955–1977, 2016.

Hu, W. W., Hu, M., Yuan, B., Jimenez, J. L., Tang, Q., Peng, J. F., Hu, W., Shao, M., Wang, M., Zeng, L. M., Wu, Y. S., Gong, Z. H., Huang, X. F. and He, L. Y.: Insights on organic aerosol aging and the influence of coal combustion at a regional receptor site of central eastern China, Atmos. Chem. Phys., 13(19), 10095–10112, 2013.

IHME: Global Burden of Disease Study 2015 (GBD 2015) Data Resources, GHDx [online] Available from: http://ghdx.healthdata.org/gbd-2015 (Accessed 2019), 2016.

Jaeglé, L., Quinn, P. K., Bates, T. S., Alexander, B. and Lin, J.-T.: Global distribution of sea salt aerosols: new constraints from in situ and remote sensing observations, Atmos. Chem. Phys., 11(7), 3137–3157, 2011.

Janssen, R. H. H., Tsimpidi, A. P., Karydis, V. A., Pozzer, A., Lelieveld, J., Crippa, M., Prévôt, A. S. H., Ait-Helal, W., Borbon, A., Sauvage, S. and Locoge, N.: Influence of local production and vertical transport on the organic aerosol budget over Paris, J. Geophys. Res. D: Atmos., 122(15), 8276–8296, 2017.

Janssens-Maenhout, G., Crippa, M., Guizzardi, D., Dentener, F., Muntean, M., Pouliot, G., Keating, T., Zhang, Q., Kurokawa, J., Wankmüller, R., Denier van der Gon, H., Kuenen, J. J. P., Klimont, Z., Frost, G., Darras, S., Koffi, B. and Li, M.: HTAP_v2.2: a mosaic of regional and global emission grid maps for 2008 and 2010 to study hemispheric transport of air pollution, Atmos. Chem. Phys., 15(19), 11411–11432, 2015.

Jathar, S. H., Gordon, T. D., Hennigan, C. J., Pye, H. O. T., Pouliot, G., Adams, P. J., Donahue, N. M. and Robinson, A. L.: Unspeciated organic emissions from combustion sources and their influence on the secondary organic aerosol budget in the United States, Proc. Natl. Acad. Sci. U. S. A., 111(29), 10473–10478, 2014.

Jena, C., Ghude, S. D., Kulkarni, R., Debnath, S., Kumar, R., Soni, V. K., Acharja, P., Kulkarni, S. H., Khare, M., Kaginalkar, A. J., Chate, D. M., Ali, K., Nanjundiah, R. S. and Rajeevan, M. N.: Evaluating the sensitivity of fine particulate matter ($PM_{2.5}$) simulations to chemical mechanism in Delhi, Atmos. Chem. Phys. Discuss., doi:10.5194/acp-2020-673, 2020.

Jimenez, J. L., Canagaratna, M. R., Donahue, N. M., Prevot, A. S. H., Zhang, Q., Kroll, J. H., DeCarlo, P. F., Allan, J. D., Coe, H., Ng, N. L., Aiken, A. C., Docherty, K. S., Ulbrich, I. M., Grieshop, A. P., Robinson, A. L., Duplissy, J., Smith, J. D., Wilson, K. R., Lanz, V. A., Hueglin, C., Sun, Y. L., Tian, J., Laaksonen, A., Raatikainen, T., Rautiainen, J., Vaattovaara, P., Ehn, M., Kulmala, M., Tomlinson, J. M., Collins, D. R., Cubison, M. J., Dunlea, E. J., Huffman, J. A., Onasch, T. B., Alfarra, M. R., Williams, P. I., Bower, K., Kondo, Y., Schneider, J., Drewnick, F., Borrmann, S., Weimer, S., Demerjian, K., Salcedo, D., Cottrell, L., Griffin, R., Takami, A., Miyoshi, T., Hatakeyama, S., Shimono, A., Sun, J. Y., Zhang, Y. M., Dzepina, K., Kimmel, J. R., Sueper, D., Jayne, J. T., Herndon, S. C., Trimborn, A. M., Williams, L. R., Wood, E. C., Middlebrook, A. M., Kolb, C. E., Baltensperger, U. and Worsnop, D. R.: Evolution of organic aerosols in the atmosphere, Science, 326(5959), 1525–1529, 2009.

Khare, P. and Gentner, D. R.: Considering the future of anthropogenic gas-phase organic compound emissions and the increasing influence of non-combustion sources on urban air quality, Atmos. Chem. Phys., 18(8), 5391–5413, 2018.

Kleinman, L. I., Daum, P. H., Lee, Y.-N., Senum, G. I., Springston, S. R., Wang, J., Berkowitz, C., Hubbe, J., Zaveri, R. A., Brechtel, F. J., Jayne, J., Onasch, T. B. and Worsnop, D.: Aircraft observations of aerosol composition and ageing in New England and Mid-Atlantic States during the summer 2002 New England Air Quality Study field campaign, J. Geophys. Res. D: Atmos., 112(D9), D09310, 2007.

Kondo, Y., Morino, Y., Fukuda, M., Kanaya, Y., Miyazaki, Y., Takegawa, N., Tanimoto, H., McKenzie, R., Johnston, P., Blake, D. R., Murayama, T. and Koike, M.: Formation and transport of oxidized reactive nitrogen, ozone, and secondary organic aerosol in Tokyo, J. Geophys. Res. D: Atmos., 113(D21), D21310, 2008.

Koo, B., Knipping, E. and Yarwood, G.: 1.5-Dimensional volatility basis set approach for modeling organic aerosol in CAMx and CMAQ, Atmos. Environ., 95, 158–164, 2014.

Krewski, D., Jerrett, M., Burnett, R. T., Ma, R., Hughes, E., Shi, Y., Turner, M. C., Arden, C., Thurston, G., Calle, E. E., Thun, M. J., Beckerman, B., Deluca, P., Finkelstein, N., Ito, K., Moore, D. K., Newbold, K. B., Ramsay, T., Ross, Z., Shin, H. and Tempalski, B.: Extended Follow-Up and Spatial Analysis of the American Cancer Society Study Linking Particulate Air Pollution and Mortality Number 140 May 2009 PRESS VERSION., 2009.

Kuwata, M., Zorn, S. R. and Martin, S. T.: Using Elemental Ratios to Predict the Density of Organic Material Composed of Carbon, Hydrogen, and Oxygen, Environ. Sci. Technol., 46(2), 787–794, 2012.

Lacey, F. G., Henze, D. K., Lee, C. J., van Donkelaar, A. and Martin, R. V.: Transient climate and ambient health impacts due to national solid fuel cookstove emissions, Proc. Natl. Acad. Sci. U. S. A., 114(6), 1269–1274, 2017.

Landrigan, P. J., Fuller, R., Acosta, N. J. R., Adeyi, O., Arnold, R., Basu, N., Baldé, A. B., Bertollini, R., Bose-O'Reilly, S., Boufford, J. I., Breysse, P. N., Chiles, T., Mahidol, C., Coll-Seck, A. M., Cropper, M. L., Fobil, J., Fuster, V., Greenstone, M., Haines, A., Hanrahan, D., Hunter, D., Khare, M., Krupnick, A., Lanphear, B., Lohani, B., Martin, K., Mathiasen, K. V., McTeer, M. A., Murray, C. J. L., Ndahimananjara, J. D., Perera, F., Potočnik, J., Preker, A. S., Ramesh, J., Rockström, J., Salinas, C., Samson, L. D., Sandilya, K., Sly, P. D., Smith, K. R., Steiner, A., Stewart, R. B., Suk, W. A., van Schayck, O. C. P., Yadama, G. N., Yumkella, K. and Zhong, M.: The Lancet Commission on pollution and health, Lancet, 391(10119), 462–512, 2018.

Lelieveld, J., Evans, J. S., Fnais, M., Giannadaki, D. and Pozzer, A.: The contribution of outdoor air pollution sources to premature mortality on a global scale, Nature, 525(7569), 367–371, 2015.

Liao, J., Hanisco, T. F., Wolfe, G. M., St. Clair, J., Jimenez, J. L., Campuzano-Jost, P., Nault, B. A., Fried, A., Marais, E. A., Gonzalez Abad, G., Chance, K., Jethva, H. T., Ryerson, T. B., Warneke, C. and Wisthaler, A.: Towards a satellite formaldehyde – in situ hybrid estimate for organic aerosol abundance, Atmos. Chem. Phys., 19(5), 2765–2785, 2019.

Li, M., Liu, H., Geng, G., Hong, C., Liu, F., Song, Y., Tong, D., Zheng, B., Cui, H., Man, H., Zhang, Q. and He, K.: Anthropogenic emission inventories in China: a review, Natl Sci Rev, 4(6), 834–866, 2017.

Li, M., Zhang, Q., Zheng, B., Tong, D., Lei, Y., Liu, F., Chaopeng, H., Kang, S., Yan, L., Zhang, Y., Bo, Y., Su, H., Cheng, Y. and He, K.: Persistent growth of anthropogenic non-methane volatile organic compound (NMVOC) emissions in China during 1990-2017: drivers, speciation and ozone formation potential, Atmos. Chem. Phys., 19, 8897–8913, 2019.

Liu, F., Zhang, Q., Tong, D., Zheng, B., Li, M., Huo, H. and He, K. B.: High-resolution inventory of technologies, activities, and emissions of coal-fired power plants in China from 1990 to 2010, Atmos. Chem. Phys., 15(23), 13299–13317, 2015.

Lu, Q., Zhao, Y. and Robinson, A. L.: Comprehensive organic emission profiles for gasoline, diesel, and gas-turbine engines including intermediate and semi-volatile organic compound emissions, Atmos. Chem. Phys., 18, 17637–17654, 2018.

Ma, P. K., Zhao, Y., Robinson, A. L., Worton, D. R., Goldstein, A. H., Ortega, A. M., Jimenez, J. L., Zotter, P., Prévôt, A. S. H., Szidat, S. and Hayes, P. L.: Evaluating the impact of new observational constraints on P-S/IVOC emissions, multi-generation oxidation, and chamber wall losses on SOA modeling for Los Angeles, CA, Atmos. Chem. Phys., 17(15), 9237–9259, 2017.

Marais, E. A., Jacob, D. J., Jimenez, J. L., Campuzano-Jost, P., Day, D. A., Hu, W., Krechmer, J., Zhu, L., Kim, P. S., Miller, C. C., Fisher, J. A., Travis, K., Yu, K., Hanisco, T. F., Wolfe, G. M., Arkinson, H. L., Pye, H. O. T., Froyd, K. D., Liao, J. and McNeill, V. F.: Aqueous-phase mechanism for secondary organic aerosol formation from isoprene: application to the southeast United States and co-benefit of SO_2 emission controls, Atmos. Chem. Phys., 16(3), 1603–1618, 2016.

McDonald, B. C., de Gouw, J. A., Gilman, J. B., Jathar, S. H., Akherati, A., Cappa, C. D., Jimenez, J. L., Lee-Taylor, J., Hayes, P. L., McKeen, S. A., Cui, Y. Y., Kim, S.-W., Gentner, D. R., Isaacman-VanWertz, G., Goldstein, A. H., Harley, R. A., Frost, G. J., Roberts, J. M., Ryerson, T. B. and Trainer, M.: Volatile chemical products emerging as largest petrochemical source of urban organic emissions, Science, 359(6377), 760–764, 2018.

Miyakawa, T., Takegawa, N. and Kondo, Y.: Photochemical evolution of submicron aerosol chemical composition in the Tokyo megacity region in summer, J. Geophys. Res. D: Atmos., 113(D14), D14304, 2008.

Molina, L. T., Kolb, C. E., de Foy, B., Lamb, B. K., Brune, W. H., Jimenez, J. L., Ramos-Villegas, R., Sarmiento, J., Paramo-Figueroa, V. H., Cardenas, B., Gutierrez-Avedoy, V. and Molina, M. J.: Air quality in North America’s most populous city – overview of the MCMA-2003 campaign, Atmos. Chem. Phys., 7(10), 2447–2473, 2007.

Molina, L. T., Madronich, S., Gaffney, J. S., Apel, E., de Foy, B., Fast, J., Ferrare, R., Herndon, S., Jimenez, J. L., Lamb, B., Osornio-Vargas, A. R., Russell, P., Schauer, J. J., Stevens, P. S., Volkamer, R. and Zavala, M.: An overview of the MILAGRO 2006 Campaign: Mexico City emissions and their transport and transformation, Atmos. Chem. Phys., 10(18), 8697–8760, 2010.

Morino, Y., Tanabe, K., Sato, K. and Ohara, T.: Secondary organic aerosol model intercomparison based on secondary organic aerosol to odd oxygen ratio in Tokyo, J. Geophys. Res.: Atmos., 119(23), 13,489–13,505, 2014.

Nault, B. A., Campuzano-Jost, P., Day, D. A., Schroder, J. C., Anderson, B., Beyersdorf, A. J., Blake, D. R., Brune, W. H., Choi, Y., Corr, C. A., de Gouw, J. A., Dibb, J., DiGangi, J. P., Diskin, G. S., Fried, A., Huey, L. G., Kim, M. J., Knote, C. J., Lamb, K. D., Lee, T., Park, T., Pusede, S. E., Scheuer, E., Thornhill, K. L., Woo, J.-H. and Jimenez, J. L.: Secondary Organic Aerosol Production from Local Emissions Dominates the Organic Aerosol Budget over Seoul, South Korea, during KORUS-AQ, Atmos. Chem. Phys., 18, 17769–17800, 2018.

Pai, S. J., Heald, C. L., Pierce, J. R., Farina, S. C., Marais, E. A., Jimenez, J. L., Campuzano-Jost, P., Nault, B. A., Middlebrook, A. M., Coe, H., Shilling, J. E., Bahreini, R., Dingle, J. H. and Vu, K.: An evaluation of global organic aerosol schemes using airborne observations, Atmos. Chem. Phys., 20(5), 2637–2665, 2020.

Pankow, J. F. and Asher, W. E.: SIMPOL.1: a simple group contribution method for predicting vapor pressures and enthalpies of vaporization of multifunctional organic compounds, Atmos. Chem. Phys., 8(10), 2773–2796, 2008.

Park, R. J., Jacob, D. J., Palmer, P. I., Clarke, A. D., Weber, R. J., Zondlo, M. A., Eisele, F. L., Bandy, A. R., Thornton, D. C., Sachse, G. W. and Bond, T. C.: Export efficiency of black carbon aerosol in continental outflow: Global implications, J. Geophys. Res. D: Atmos., 110(D11), D11205, 2005.

Park, R. J., Jacob, D. J., Kumar, N. and Yantosca, R. M.: Regional visibility statistics in the United States: Natural and transboundary pollution influences, and implications for the Regional Haze Rule, Atmos. Environ., 40(28), 5405–5423, 2006.

Parrish, D. D., Kuster, W. C., Shao, M., Yokouchi, Y., Kondo, Y., Goldan, P. D., de Gouw, J. A., Koike, M. and Shirai, T.: Comparison of air pollutant emissions among mega-cities, Atmos. Environ., 43(40), 6435–6441, 2009.

Peng, Z. and Jimenez, J. L.: KinSim: A Research-Grade, User-Friendly, Visual Kinetics Simulator for Chemical-Kinetics and Environmental-Chemistry Teaching, J. Chem. Educ., 96(4), 806–811, 2019.

Platt, S. M., Haddad, I. E., Pieber, S. M., Huang, R.-J., Zardini, A. A., Clairotte, M., Suarez-Bertoa, R., Barmet, P., Pfaffenberger, L., Wolf, R., Slowik, J. G., Fuller, S. J., Kalberer, M., Chirico, R., Dommen, J., Astorga, C., Zimmermann, R., Marchand, N., Hellebust, S., Temime-Roussel, B., Baltensperger, U. and Prévôt, A. S. H.: Two-stroke scooters are a dominant source of air pollution in many cities, Nat. Commun., 5(1), 3749, 2014.

Pollack, I. B., Ryerson, T. B., Trainer, M., Neuman, J. A., Roberts, J. M. and Parrish, D. D.: Trends in ozone, its precursors, and related secondary oxidation products in Los Angeles, California: A synthesis of measurements from 1960 to 2010, J. Geophys. Res. D: Atmos., 118(11), 5893–5911, 2013.

Punger, E. M. and West, J. J.: The effect of grid resolution on estimates of the burden of ozone and fine particulate matter on premature mortality in the USA, Air Qual. Atmos. Health, 6(3),

563–573, 2013.

Pye, H. O. T. and Seinfeld, J. H.: A global perspective on aerosol from low-volatility organic compounds, Atmos. Chem. Phys., 10, 4377–4401, 2010.

Ridley, D. A., Heald, C. L., Ridley, K. J. and Kroll, J. H.: Causes and consequences of decreasing atmospheric organic aerosol in the United States, Proc. Natl. Acad. Sci. U. S. A., 115(2), 290–295, 2018.

Robinson, A. L., Donahue, N. M., Shrivastava, M. K., Weitkamp, E. A., Sage, A. M., Grieshop, A. P., Lane, T. E., Pierce, J. R. and Pandis, S. N.: Rethinking Organic Aerosols: Semivolatile Emissions and Photochemical Aging, Science, 315(5816), 1259–1262, 2007.

Rumble, J. R., Ed.: CRC Handbook of Chemistry and Physics, 100th Edition, 2019 - 2020, Taylor & Francis Group., 2019.

Ryerson, T. B., Andrews, A. E., Angevine, W. M., Bates, T. S., Brock, C. A., Cairns, B., Cohen, R. C., Cooper, O. R., de Gouw, J. A., Fehsenfeld, F. C., Ferrare, R. A., Fischer, M. L., Flagan, R. C., Goldstein, A. H., Hair, J. W., Hardesty, R. M., Hostetler, C. A., Jimenez, J. L., Langford, A. O., McCauley, E., McKeen, S. A., Molina, L. T., Nenes, A., Oltmans, S. J., Parrish, D. D., Pederson, J. R., Pierce, R. B., Prather, K., Quinn, P. K., Seinfeld, J. H., Senff, C. J., Sorooshian, A., Stutz, J., Surratt, J. D., Trainer, M., Volkamer, R., Williams, E. J. and Wofsy, S. C.: The 2010 California Research at the Nexus of Air Quality and Climate Change (CalNex) field study, J. Geophys. Res. D: Atmos., 118(11), 5830–5866, 2013.

Sacks, J., Buckley, B., Alexis, N., Angrish, M., Beardslee, R., Benson, A., Brown, J., Buckley, B., Campen, M., Chan, E., Coffman, E., Davis, A., Dutton, S. J., Eftim, S., Gandy, J., Hemming, B. L., Hines, E., Holliday, K., Kerminen, V.-M., Kiomourtzoglou, M.-A., Kirrane, E., Kotchmar, D., Koturbash, I., Kulmala, M., Lassiter, M., Limaye, V., Ljungman, P., Long, T., Luben, T., Malm, W., McDonald, J. F., McDow, S., Mickley, L., Mikati, I., Mulholland, J., Nichols, J., Patel, M. M., Pinder, R., Pinto, J. P., Rappazzo, K., Richomond-Bryant, J., Rosa, M., Russell, A., Schichtel, B., Stewart, M., Stanek, L. W., Turner, M., Van Winkle, L., Wagner, J., Weaver, Christopher, Wellenius, G., Whitsel, E., Yeckel, C., Zanobetti, A. and Zhang, M.: Integrated Science Assessment (ISA) for Particulate Matter (Final Report, Dec 2019), Environmental Protection Agency. [online] Available from: https://cfpub.epa.gov/ncea/isa/recordisplay.cfm?deid=347534 (Accessed 20 October 2020), 2019.

Schroder, J. C., Campuzano-Jost, P., Day, D. A., Shah, V., Larson, K., Sommers, J. M., Sullivan, A. P., Campos, T., Reeves, J. M., Hills, A., Hornbrook, R. S., Blake, N. J., Scheuer, E., Guo, H., Fibiger, D. L., McDuffie, E. E., Hayes, P. L., Weber, R. J., Dibb, J. E., Apel, E. C., Jaeglé, L., Brown, S. S., Thronton, J. A. and Jimenez, J. L.: Sources and Secondary Production of Organic Aerosols in the Northeastern US during WINTER, J. Geophys. Res. D: Atmos., doi:10.1029/2018JD028475, 2018.

Seinfeld, J. H. and Pandis, S. N.: Atmospheric Chemistry and Physics: From Air Pollution to

Climate Change, Second., John Wiley & Sons, Inc., Hoboken, NJ USA., 2006.

Shaddick, G., Thomas, M. L., Amini, H., Broday, D., Cohen, A., Frostad, J., Green, A., Gumy, S., Liu, Y., Martin, R. V., Pruss-Ustun, A., Simpson, D., van Donkelaar, A. and Brauer, M.: Data Integration for the Assessment of Population Exposure to Ambient Air Pollution for Global Burden of Disease Assessment, Environ. Sci. Technol., 52(16), 9069–9078, 2018.

Shah, V., Jaeglé, L., Thornton, J. A., Lopez-Hilfiker, F. D., Lee, B. H., Schroder, J. C., Campuzano-Jost, P., Jimenez, J. L., Guo, H., Sullivan, A. P., Weber, R. J., Green, J. R., Fiddler, M. N., Bililign, S., Campos, T. L., Stell, M., Weinheimer, A. J., Montzka, D. D. and Brown, S. S.: Chemical feedbacks weaken the wintertime response of particulate sulfate and nitrate to emissions reductions over the eastern United States, Proc. Natl. Acad. Sci. U. S. A., 115(32), 8110–8115, 2018.

Shah, V., Jaeglé, L., Jimenez, J. L., Schroder, J. C., Campuzano-Jost, P., Campos, T. L., Reeves, J. M., Stell, M., Brown, S. S., Lee, B. H., Lopez-Hilfiker, F. D. and Thornton, J. A.: Widespread Pollution from Secondary Sources of Organic Aerosols during Winter in the Northeastern United States, Geophys. Res. Lett., doi:10.1029/2018GL081530, 2019.

Shrivastava, M., Cappa, C. D., Fan, J., Goldstein, A. H., Guenther, A. B., Jimenez, J. L., Kuang, C., Laskin, A., Martin, S. T., Ng, N. L., Petaja, T., Pierce, J. R., Rasch, P. J., Roldin, P., Seinfeld, J. H., Shilling, J., Smith, J. N., Thornton, J. A., Volkamer, R., Wang, J., Worsnop, D. R., Zaveri, R. A., Zelenyuk, A. and Zhang, Q.: Recent advances in understanding secondary organic aerosol: Implications for global climate forcing, Rev. Geophys., 55(2), 509–559, 2017.

Silva, R. A., Adelman, Z., Fry, M. M. and West, J. J.: The Impact of Individual Anthropogenic Emissions Sectors on the Global Burden of Human Mortality due to Ambient Air Pollution, Environ. Health Perspect., 124(11), 1776–1784, 2016.

Singh, A., Satish, R. V. and Rastogi, N.: Characteristics and sources of fine organic aerosol over a big semi-arid urban city of western India using HR-ToF-AMS, Atmos. Environ., 208, 103–112, 2019.

Stewart, G. J., Nelson, B. S., Acton, W. J. F., Vaughan, A. R., Farren, N. J., Hopkins, J. R., Ward, M. W., Swift, S. J., Arya, R., Mondal, A., Jangirh, R., Ahlawat, S., Yadav, L., Sharma, S. K., Yunus, S. S. M., Hewitt, C. N., Nemitz, E., Mullinger, N., Gadi, R., Sahu, L. K., Tripathi, N., Rickard, A. R., Lee, J. D., Mandal, T. K. and Hamilton, J. F.: Emissions of intermediate-volatility and semi-volatile organic compounds from domestic fuels used in Delhi, India, Atmos. Chem. Phys. Discuss., doi:10.5194/acp-2020-860, 2020.

The International GEOS-Chem User Community: geoschem/geos-chem: GEOS-Chem 12.0.0 release, , doi:10.5281/ZENODO.1343547, 2018.

Toon, O. B., Maring, H., Dibb, J., Ferrare, R., Jacob, D. J., Jensen, E. J., Luo, Z. J., Mace, G. G., Pan, L. L., Pfister, L., Rosenlof, K. H., Redemann, J., Reid, J. S., Singh, H. B., Thompson, A. M., Yokelson, R., Minnis, P., Chen, G., Jucks, K. W. and Pszenny, A.: Planning, implementation, and scientific goals of the Studies of Emissions and Atmospheric Composition, Clouds and Climate Coupling by Regional Surveys ($SEAC^4RS$) field mission, J. Geophys. Res. D: Atmos., 121(9), 4967–5009, 2016.

Tsimpidi, A. P., Karydis, V. A., Zavala, M., Lei, W., Molina, L., Ulbrich, I. M., Jimenez, J. L. and Pandis, S. N.: Evaluation of the volatility basis-set approach for the simulation of organic aerosol formation in the Mexico City metropolitan area, Atmos. Chem. Phys., 10(2), 525–546, 2010.

Vaden, T. D., Imre, D., Beránek, J., Shrivastava, M. and Zelenyuk, A.: Evaporation kinetics and phase of laboratory and ambient secondary organic aerosol, Proc. Natl. Acad. Sci. U. S. A., 108(6), 2190–2195, 2011.

Wang, L., Slowik, J. G., Tripathi, N., Bhattu, D., Rai, P., Kumar, V., Vats, P., Satish, R., Baltensperger, U., Ganguly, D., Rastogi, N., Sahu, L. K., Tripathi, S. N. and Prévôt, A. S. H.: Source characterization of volatile organic compounds measured by proton-transfer-reaction time-of-flight mass spectrometers in Delhi, India, Atmos. Chem. Phys., 20(16), 9753–9770, 2020.

Wang, M., Shao, M., Chen, W., Yuan, B., Lu, S., Zhang, Q., Zeng, L. and Wang, Q.: A temporally and spatially resolved validation of emission inventories by measurements of ambient volatile organic compounds in Beijing, China, Atmos. Chem. Phys., 14(12), 5871–5891, 2014.

Wang, Y. Q., Zhang, X. Y., Sun, J. Y., Zhang, X. C., Che, H. Z. and Li, Y.: Spatial and temporal variations of the concentrations of PM_{10}, $PM_{2.5}$ and PM_1 in China, Atmos. Chem. Phys., 15, 13585–13598, 2015.

Warneke, C., McKeen, S. A., de Gouw, J. A., Goldan, P. D., Kuster, W. C., Holloway, J. S., Williams, E. J., Lerner, B. M., Parrish, D. D., Trainer, M., Fehsenfeld, F. C., Kato, S., Atlas, E. L., Baker, A. and Blake, D. R.: Determination of urban volatile organic compound emission ratios and comparison with an emissions database, J. Geophys. Res. D: Atmos., 112(D10), doi:10.1029/2006JD007930, 2007.

Warneke, C., de Gouw, J. A., Holloway, J. S., Peischl, J., Ryerson, T. B., Atlas, E., Blake, D., Trainer, M. and Parrish, D. D.: Multiyear trends in volatile organic compounds in Los Angeles, California: Five decades of decreasing emissions, J. Geophys. Res. D: Atmos., 117(D21), D00V17, 2012.

Wood, E. C., Canagaratna, M. R., Herndon, S. C., Onasch, T. B., Kolb, C. E., Worsnop, D. R., Kroll, J. H., Knighton, W. B., Seila, R., Zavala, M., Molina, L. T., Decarlo, P. F., Jimenez, J. L., Weinheimer, A. J., Knapp, D. J., Jobson, B. T., Stutz, J., Kuster, W. C. and Williams, E. J.: Investigation of the correlation between odd oxygen and secondary organic aerosol in Mexico City and Houston, Atmos. Chem. Phys., 10(18), 8947–8968, 2010.

Worton, D. R., Isaacman, G., Gentner, D. R., Dallmann, T. R., Chan, A. W. H., Ruehl, C., Kirchstetter, T. W., Wilson, K. R., Harley, R. A. and Goldstein, A. H.: Lubricating Oil Dominates Primary Organic Aerosol Emissions from Motor Vehicles, Environ. Sci. Technol., 48(7),

3698–3706, 2014.

Zhang, Q., Alfarra, M. R., Worsnop, D. R., James, D., Coe, H., Canagaratna, M. R. and Jimenez, J. L.: Deconvolution and Quantification of Hydrocarbon-like and Oxygenated Organic Aerosols Based on Aerosol Mass Spectrometry Deconvolution and Quantification of Hydrocarbon-like and Oxygenated Organic Aerosols Based on Aerosol Mass Spectrometry, Environ. Sci. Technol., 39(13), 4938–4952, 2005.

Zhang, Q., Streets, D. G., Carmichael, G. R., He, K. B., Huo, H., Kannari, A., Klimont, Z., Park, I. S., Reddy, S., Fu, J. S., Chen, D., Duan, L., Lei, Y., Wang, L. T. and Yao, Z. L.: Asian emissions in 2006 for the NASA INTEX-B mission, Atmos. Chem. Phys., 9(14), 5131–5153, 2009.

Zhang, Q. J., Beekmann, M., Freney, E., Sellegri, K., Pichon, J. M., Schwarzenboeck, A., Colomb, A., Bourrianne, T., Michoud, V. and Borbon, A.: Formation of secondary organic aerosol in the Paris pollution plume and its impact on surrounding regions, Atmos. Chem. Phys., 15(24), 13973–13992, 2015.

Zhao, Y., Hennigan, C. J., May, A. A., Daniel, S., Gouw, J. A. D., Gilman, J. B., Kuster, W. C. and Robinson, A. L.: Intermediate-Volatility Organic Compounds: A Large Source of Secondary Organic Aerosol, Environ. Sci. Technol, 48(23), 13743–13750, 2014.

Zhao, Y., Saleh, R., Saliba, G., Presto, A. A., Gordon, T. D., Drozd, G. T., Goldstein, A. H., Donahue, N. M. and Robinson, A. L.: Reducing secondary organic aerosol formation from gasoline vehicle exhaust, Proc. Natl. Acad. Sci. U. S. A., 114(27), 6984–6989, 2017.

Zheng, B., Huo, H., Zhang, Q., Yao, Z. L., Wang, X. T., Yang, X. F., Liu, H. and He, K. B.: High-resolution mapping of vehicle emissions in China in 2008, Atmos. Chem. Phys., 14(18), 9787–9805, 2014.

Zheng, B., Tong, D., Li, M., Liu, F., Hong, C., Geng, G., Li, H., Li, X., Peng, L., Qi, J., Yan, L., Zhang, Y., Zhao, H., Zheng, Y., He, K. and Zhang, Q.: Trends in China's anthropogenic emissions since 2010 as the consequence of clean air actions, Atmos. Chem. Phys., 18(19), 14095–14111, 2018.